REPORT 1052

A SUMMARY OF LATERAL-STABILITY DERIVATIVES CALCULATED FOR WING PLAN FORMS IN SUPERSONIC FLOW

By ARTHUR L. JONES and ALBERTA ALKSNE

SUMMARY

A compilation of theoretical values of the lateral-stability derivatives for wings at supersonic speeds is presented in the form of design charts. The wing plan forms for which this compilation has been prepared include a rectangular, two trapezoidal, two triangular, a fully-tapered swept-back, a swept-back hexagonal, an unswept hexagonal, and a notched triangular plan form. A full set of results, that is, values for all nine of the lateral-stability derivatives for wings, was available for the first six of these plan forms only. The reasons for the incompleteness of the results available for other plan forms are discussed.

The values of the derivatives presented were obtained directly from tabulated results in the reports referenced or were calculated from expressions presented in these reports. The expressions for the derivatives were derived using linearized theory for compressible flow. The values presented, however, do not represent exact linear-theory solutions in every case due to the fact that approximations and simplifications were sometimes necessary in the derivation of the expressions or in the calculations of the numerical results. The effects of these approximations and simplifications on the accuracy and applicability of the results are considered.

INTRODUCTION

The calculation of the lateral-stability derivative coefficients (hereinafter referred to as the lateral-stability derivatives) for thin wings at supersonic speeds has been accomplished for a number of plan forms and the results are reported in references 1 through 18. These results are necessarily incomplete in view of the fact that there is an unlimited number of plan forms that could be investigated. There appears to be a sufficient quantity of results available, however, to warrant the preparation of a summary. In fact, some summaries, such as references 10 and 17, are already available but the results presented in these reports are restricted to a fairly small number of plan forms or to a small number of derivatives. It is the purpose of this report, therefore, to assemble and present a more extensive set of numerical results than was heretofore available. These results will be limited to the thin-airfoil, inviscid-flow solutions obtained from application of the linearized theory of compressible flow. They will be presented in the form of design charts showing the variations of the derivatives [1] with Mach number, aspect ratio, and other plan-form parameters. The derivatives have been evaluated in a manner that permits their direct application in an analysis using the stability axes system.

A discussion of the limitations in the applicability and availability of the lateral-stability derivative results is included. Some of the limitations are inherent in the linearized theory itself, but most of the limitations are due to the approximations and simplifications sometimes found necessary in the application of the theory.

The plan forms for which the results are presented are illustrated in figure 1. Included are a rectangular, two

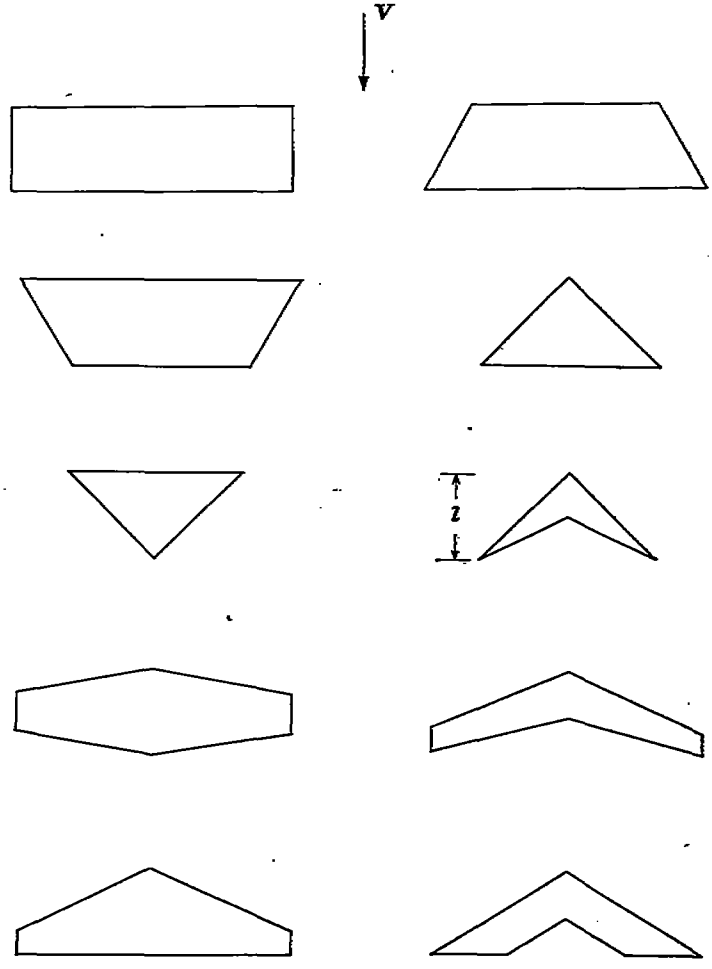

FIGURE 1.—Types of plan forms for which summarized results are presented.

[1] Although the scale labels show that some of the stability derivatives presented in the figures are divided by angle of attack or angle of attack squared, reference to the variation of this quotient with other variables will be simply referred to as the variation of the derivative. This usage is consistent with the terminology used in previous NACA reports.

triangular, two trapezoidal, a fully-tapered swept-back, a swept-back hexagonal, an unswept hexagonal, and a notched triangular plan form. This group may not cover all the plan forms for which at least partially complete results are available. It is, however, a fairly representative group. In table I the sources of the results for the lateral-stability derivatives of the plan forms surveyed are listed.

SYMBOLS AND COEFFICIENTS

A aspect ratio

b span of wing measured normal to plane of symmetry

B $\sqrt{M^2-1}$

c_r chord of wing root

$c.\ g.$ center of gravity

C_l rolling-moment coefficient $\left(\frac{L}{qSb}\right)$

C_n yawing-moment coefficient $\left(\frac{N}{qSb}\right)$

C_Y side-force coefficient $\left(\frac{Y}{qS}\right)$

C_{l_p} damping-in-roll derivative $\left[\frac{\partial C_l}{\partial(pb/2V)}\right]$

C_{l_r} rolling-moment-due-to-yawing derivative $\left[\frac{\partial C_l}{\partial(rb/2V)}\right]$

C_{l_β} rolling-moment-due-to-sideslip derivative $\left(\frac{\partial C_l}{\partial\beta}\right)$

C_{n_p} yawing-moment-due-to-rolling derivative $\left[\frac{\partial C_n}{\partial(pb/2V)}\right]$

C_{n_r} yawing-moment-due-to-yawing derivative $\left[\frac{\partial C_n}{\partial(rb/2V)}\right]$

C_{n_β} yawing-moment-due-to-sideslip derivative $\left(\frac{\partial C_n}{\partial\beta}\right)$

C_{Y_p} side-force-due-to-rolling derivative $\left[\frac{\partial C_Y}{\partial(pb/2V)}\right]$

C_{Y_r} side-force-due-to-yawing derivative $\left[\frac{\partial C_Y}{\partial(rb/2V)}\right]$

C_{Y_β} side-force-due-to-sideslip derivative $\left(\frac{\partial C_Y}{\partial\beta}\right)$

l over-all longitudinal length of swept-back wing (See fig. 1.)

$l_{c.\ g.}$ longitudinal location of center of gravity aft of the leading edge of the root chord

L rolling moment (See fig. 2(b).)

m slope of right wing tip or leading edge relative to plane of symmetry (Positive for raked-out tip, negative for raked-in tip.)

M free-stream Mach number

N yawing moment (See fig. 2(b).)

p rate of roll, radians per second

q free-stream dynamic pressure

r rate of yaw, radians per second

S area of wing

V free-stream velocity

x longitudinal coordinate

$x_{c.\ g.}$ arbitrary longitudinal location of the center of gravity with respect to the location specified in this report (Positive for locations forward of those specified.)

y lateral coordinate

Y side force (See fig. 2 (b).)

z vertical coordinate

α angle of attack, radians

β angle of sideslip (positive when sideslipping to right), degrees

λ taper ratio

AXES

At least three systems of axes are associated with the development and application of stability derivatives. For instance, the theoretical expressions for the stability derivatives are most easily derived using a set of three orthogonal axes, known as the wind axes, that are oriented as shown in figure 2 (a). The origin of these axes is at the leading edge of the root chord. The x axis is an extension of the free-stream vector through the origin and is positive rearward. The y axis lies in the plane of the wing perpendicular to the x axis and is positive toward the right tip. The z axis stands perpendicular to the x and y axes and is positive upward. These axes are commonly used in wing-theory calculations.

Body-axes systems (see fig. 2 (b)) are sometimes used in the calculations of the motion of an aircraft. These calculations are commonly referred to as dynamic-stability calculations. The origin of the axes for such calculations is usually the center of gravity rather than the leading edge of the root chord. Thus the expressions initially derived for the derivatives should be corrected for the change in moment-center location accompanying the change in location of the origin of the body axes.

A third system of axes known as the stability axes (fig. 2 (c)) is often preferred for dynamic-stability calculations. The basic difference between the orientations of a stability-axes system and a body-axes system is the location of the x axis. In a stability-axes system the x axis is assumed to lie along the intersection of the plane of symmetry and a plane perpendicular to the plane of symmetry which contains the free-stream velocity vector (or the velocity vector of the center of gravity). Thus the stability axes, in general, correspond to the body axes rotated through an angle of $-\alpha$ and, in order to transform expressions for stability derivatives that are applicable to a body-axes system to expressions applicable to a stability-axes system, it is necessary to correct for the angle of attack. If the origins of the body and stability axes are coincident, this correction can be made by using the transformation formulas in reference 19. If the origins are not coincident, the correction must also include the effects of the chordwise distance between the origins. Most of the reports used as sources for the material presented, references 1 through 17, provide either formulas for both systems of axes or means for converting from one system to the other. It is interesting to note that the definitions of the positive directions for the velocities, forces, and moments of the wing conform to the right hand screw-rule for a set of body or stability axes.

For the calculation of the stability derivatives presented herein, the location of the center of gravity was selected as $c_r/2$ for the rectangular, trapezoidal, and unswept hexagonal wings, (2/3) c_r for the triangular wings, and (2/3) l for the swept-back wings. The values of the derivatives pertain to a stability-axes system so located. For arbitrary locations

of the center of gravity the derivatives that are affected by changes in the location can be evaluated using the following formulas:

$$(C_{l_r})_{x_{c.g.}}=C_{l_r}-\frac{2x_{c.g.}}{b}C_{l_\beta}$$

$$(C_{n_p})_{x_{c.g.}}=C_{n_p}-\frac{x_{c.g.}}{b}C_{Y_p}$$

$$(C_{n_\beta})_{x_{c.g.}}=C_{n_\beta}-\frac{x_{c.g.}}{b}C_{Y_\beta}$$

$$(C_{n_r})_{x_{c.g.}}=C_{n_r}-\frac{x_{c.g.}}{b}\left(C_{Y_r}+2C_{n_\beta}-2\frac{x_{c.g.}}{b}C_{Y_\beta}\right)$$

$$(C_{Y_r})_{x_{c.g.}}=C_{Y_r}-\frac{2x_{c.g.}}{b}C_{Y_\beta}$$

DERIVATION OF RESULTS

The derivation of theoretical results involves both the formulation of expressions for the derivatives and the calculation of the numerical values of the derivatives for specific plan forms and conditions. In some of the reports referenced, the analytical expressions for the derivatives were derived and presented but no numerical results were included. In other reports, both the analytical expressions and a few numerical results were given. The following discussion, therefore, will be concerned with the general method of analysis used in obtaining the analytical expressions and the way in which the numerical results presented were compiled.

GENERAL METHOD OF ANALYSIS

A stability derivative is an expression of the rate of change of a force or moment with respect to the motion producing it. Once the shape of the object for which a stability derivative is desired has been decided upon and its motion prescribed, an analysis to determine the resulting force or moment can be started. The first step in the analysis is the formulation of the boundary conditions and at this point an idealization is usually made. For a wing of finite dimensions it is convenient to assume that the effects of wing thickness and of the viscosity of the flow can be ignored or at least estimated independently. On the basis of this assumption, the wing and its flow field can be represented by a thin plate operating in an inviscid flow. This idealization permits the linearized theory for compressible flow to be used for the analysis, provided the angle of attack of the wing is kept small.

The first step in the calculation of the lateral-stability derivatives for a wing, therefore, is the specification of boundary conditions for a thin wing in sideslip, roll, or yaw. This specification can be made readily for two of these three lateral motions. For instance, a wing in sideslip at a small angle of attack can be represented by a flat plate in the same position and the plate can be simulated by use of a uniform distribution of the vertical perturbation velocity over the plan form. A rolling wing can be represented by a twisted thin plate and simulated by a linear spanwise variation of the downwash perturbation velocity over the plan-form area. This representation of the rolling wing is an illustration of the manner in which quasi-steady flow conditions can be substituted for conditions that are, in fact, unsteady. Such a substitution permits the use of a simple steady-state analysis which yields results of sufficient accuracy for the motions considered in stability theory if not for the more rapid motions involved in flutter theory. A yawing wing, however, cannot be suitably represented by a flat or twisted thin plate in steady flow. In fact, no quasi-steady flow conditions have been developed at the present time which would permit the straightforward application of a steady-state analysis. Thus it appears that the most desirable procedure in the case of the yawing wing would be to undertake the analysis as a problem in unsteady flow. Such analyses are quite complex, however, and have not as

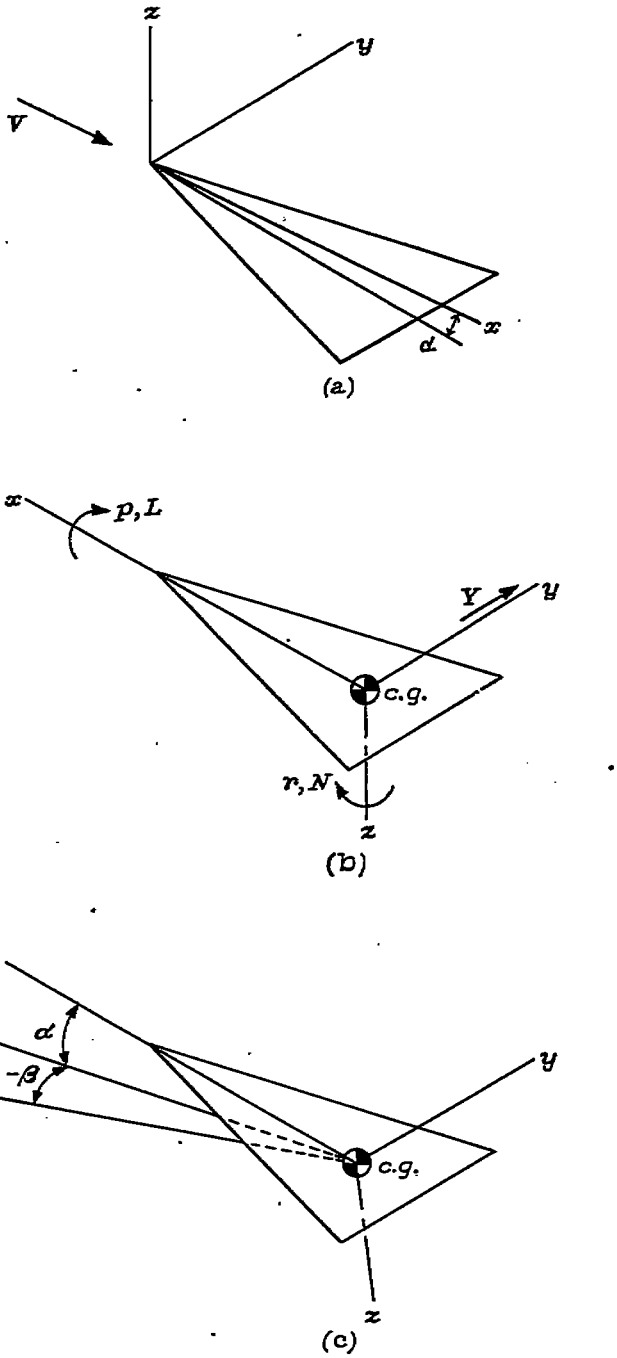

(a) Wind-axes system used in derivations of expressions for stability derivatives;
(b) Body-axes system and definition of positive moments and velocities;
(c) Stability-axes system usually preferred for dynamic-stability calculations.

FIGURE 2.—Three systems of axes associated with the development and application of stability derivatives.

yet been carried out extensively. Consequently, the results presented herein for the derivatives due to yawing are approximations based on strip theory. In the case of the rectangular plan form of infinite span or the trapezoidal plan form with raked-in supersonic tips, the validity of these results has been confirmed by an unsteady-flow solution presented in reference 20.

Having specified the boundary conditions, the next step in the analysis is to apply the linearized theory for compressible flow to the calculation of the pressure distributions. The details of this step may be found in a number of reports dealing with supersonic wing theory. (See, for example, references 21, 22, and 23.) Unfortunately, only pressures acting normal to the surface of the flat plate are calculated directly from the application of the linearized theory. These pressures are not a complete representation of the pressures acting on a wing of finite thickness, and in order to obtain a better representation the theory of edge suction must be applied and the pressures acting on the edges of the thin plate determined. Then by using both the normal and edge pressures, the moments and forces acting on the wing can be determined for the motion prescribed and the stability derivative can be calculated.

The foregoing general description of the method of calculating stability derivatives for wings, using the linearized theory of compressible flow, is merely a brief summarization of the procedure. For a more detailed description of the steps involved, the reports referenced should be consulted.

LIMITATIONS OF BASIC THEORY

The idealization of the flow field discussed above and the resulting simplifications in the theoretical analysis are reflected as limitations in the applicability of the results obtained in this manner. An obvious limitation, for instance, is that the results should be applicable only at the small angles of attack to which the wing was restricted for the analysis. Comparisons of experimental and theoretical results, however, have shown that this particular limitation usually can be exceeded in practical applications without incurring excessive inaccuracy. The less obvious limitations can be deduced from considerations of the effects of neglecting thickness and viscosity. For instance, the two basic reasons for differences between the experimental and theoretical results are: (1) the difference in pressure distributions caused by neglecting the effects of thickness, camber, and viscosity in the calculations; and (2) the existence of a skin-friction force caused by viscosity. In general, it does not seem likely that the pressure distributions due to thickness or camber will vary appreciably with any of these lateral motions. Consequently the linearized-theory results should not be greatly limited in application due to the effects of thickness or camber. On the other hand, the effect of viscosity on the pressure distribution, which is principally the effect of the boundary layer, is of consequence. It is very difficult, however, to determine the nature of the boundary-layer flow and its effect on the pressure distribution in steady straight flight and even more difficult in the case of flight involving the lateral motions. Thus the contribution of the pressure-distribution effects of viscosity to the values of the lateral-stability derivatives is a relatively unknown factor and probably the greatest source of discrepancy between the theoretical and actual values of the lateral derivatives. The skin-friction force, which is also due to viscosity, will vary appreciably with yawing velocity but not significantly with rolling velocity or sideslip. The effects of this force can be estimated and added to the linearized-theory value of C_{n_r} to reduce the limitations of applicability of this derivative. The contribution of the skin-friction force to C_{l_r}, however, is not significant since it is mainly a drag force and has only a very small component in the direction that would produce a rolling moment.

Another assumption which is inherent in the analysis applied is that the wing be completely rigid. The applicability of the theoretical results obtained on the basis of complete rigidity is limited, of course, by the effects of the deflection or distortion of the actual wing. However, only wings that have exceptionally long and slender panel lengths are subject to much distortion or deflection. Furthermore, current studies of the effect of aeroelasticity on stability derivatives are directed toward the determination of deviations from rigid-body results and it can be anticipated that the possibility of making appropriate changes in the values of the derivatives given herein may result from such analyses.

COMPILATION OF NUMERICAL RESULTS

The numerical results presented were obtained directly from the results tabulated in references 1 through 17 or were calculated using expressions presented in these reports. Wherever possible, both the numerical values of the derivatives and the expressions from which they were obtained were checked against identical results available from duplicate analyses. The plotting and cross plotting of the results in the construction of the figures presented also provided an effective check against errors.

Use was made of the reversability theorem (see reference 24) in the calculation and checking of the results for the damping-in-roll derivative C_{l_p}. No evidence or proof exists, however, that would permit the reversability theorem to be applied to the calculation or checking of the results for the other lateral derivatives.

RESULTS AND DISCUSSION

PRESENTATION OF RESULTS

As mentioned previously, the plan forms covered in this summary include a rectangular, two triangular, two trapezoidal, a fully-tapered swept-back, a swept-back hexagonal, an unswept hexagonal, and a notched triangular plan form. Estimates of all the lateral stability derivatives are available for the first six of these plan forms. Only partially complete results are available for the other plan forms.

The values of the derivatives plotted against aspect ratio and against Mach number parameter B are shown in figures 3 through 19. The results are grouped by derivatives rather than by plan forms. The values of the damping-in-roll parameter BC_{l_p} for all the plan forms surveyed are presented in figures 3 and 4, which show the variation of this derivative with the aspect-ratio parameter BA. A similar presentation,

figure 7, was used for the side-force derivative C_{Y_p}. The other derivatives required separate plots to show the aspect-ratio and Mach number variations for each type of plan form. In table II, a convenient cross reference of the figure numbers, plan forms, and derivatives is presented.

For these general results, the aspect-ratio range investigated extended from 0 to 9 and values of the derivatives were calculated for constant values of B of 1, 2, and 4. The Mach number parameter range investigated extended from 0 to 4, corresponding to Mach numbers of 1 and 4.13, respectively, and the derivatives were calculated for aspect ratios of 2, 4, and 6. More extensive ranges and additional intermediate values of these variables could have been investigated, but the complexity of the calculations made it impractical to do so. It is felt, however, that included within these limits of aspect ratio and Mach number are most of the plan forms and speeds currently of interest. Furthermore, by interpolation and, in some instances, by careful extrapolation of the results presented, it is possible to obtain theoretical values of the derivatives for plan forms of the type covered, but not specifically investigated, that should be useful as preliminary design estimates.

For the trapezoidal plan forms, the tip rake was selected to correspond to an angle of sweep of approximately 63° ($m=\pm 0.5$) and the aspect ratio was varied by changing the span. Supplementary plots showing the variation of the derivatives with tip rake for a constant aspect ratio are presented in figures 20 through 28. For the fully-tapered swept-back plan forms, the value of the ratio of the root chord to over-all length c_r/l was set at 0.5 and the aspect ratio was varied by changing the sweep of the leading edge. Supplementary plots were used in this case to show the variation of the derivatives with the ratio of root chord to the over-all length for a constant value of leading-edge sweep. These variations are presented in figures 29 through 37.

In figures 38 through 67 the variations with taper ratio and with leading-edge slope of the derivatives available for the swept-back and unswept hexagonal and the notched triangular plan forms are presented.

ASPECT RATIO AND MACH NUMBER RANGES COVERED

In many instances, the results previously described were available only within small portions of the ranges of aspect ratio and Mach number mentioned. The reasons for these limitations are discussed in the following paragraphs of this section.

For the lateral motions of rolling and sideslip, the linearized theory is directly applicable and the results available are limited only by the complexity of the calculations involved in determining the load distributions for certain plan forms and certain conditions. For the yawing motions, however, the difficulty in specifying quasi-steady boundary conditions precludes the direct application of steady-state linearized theory. Approximate solutions based on strip theory can be used, however, wherever suitable solutions of this type can be developed. Rigorous unsteady-flow solutions would of course be preferable for the yawing derivatives but only one such solution has been reported at this time. Thus it is apparent that the derivatives due to yawing are neither as available nor as generally applicable as the derivatives due to rolling or sideslip.

The cause of the calculation complexities that limit the determination of the load distribution to certain plan forms and certain conditions is the existence of regions on a wing which are affected by the interaction of flows past two or more subsonic edges [2] lying within the Mach forecones of points contained within the region. Such regions exist on any wing having interacting subsonic edges, that is, on any wing having one subsonic edge lying within the region of influence of another. These regions also exist on a wing having mutually interacting subsonic edges. The determination of the load distribution for such regions is extremely difficult using the basic integral-equation methods (references 21 and 22) developed for supersonic wing theory. This is especially true for the regions influenced by mutually interacting subsonic edges. As a consequence, special cancellation-of-load techniques have been used (references 11, 15, and 18) to handle plan forms having interacting or mutually interacting subsonic edges. The application of these cancellation techniques, however, usually involves rather lengthy calculations and, consequently, numerical results are available for only relatively few of the plan forms that require such methods. Thus most of the results presented herein are for plan forms that do not have interacting subsonic edges.

The actual ranges of the aspect-ratio parameter for which results are presented are given in table III. The limits of these ranges are explained in the discussion that follows.

Rectangular plan form.—For values of BA less than 1 the Mach lines from the tip of the rectangular plan form would intersect the opposite edges and thereby change them from noninteracting to interacting subsonic edges. Thus a lower limit is set on the aspect-ratio parameter BA for which C_{l_p}, C_{n_p}, C_{Y_p}, C_{l_β}, C_{n_β}, and C_{Y_β} are presented. The derivatives due to yawing, C_{l_r}, C_{n_r}, and C_{Y_r}, were calculated using the analysis presented in reference 6. This analysis indicated that reasonably accurate approximate values of C_{l_r}, C_{n_r}, and C_{Y_r} could be obtained as a fraction $\frac{\alpha(1-B^2)}{B^2}$ of the C_{l_p}, C_{n_p}, and C_{Y_p} results. Thus the limitations of the aspect-ratio parameter for C_{l_r}, C_{n_r}, and C_{Y_r} are the same as those for C_{l_p}, C_{n_p}, and C_{Y_p}.

Trapezoidal plan form.—The lower limits on the aspect-ratio parameter for both types of trapezoidal plan form (tips raked in and tips raked out) are to prevent the plan-form tips from becoming interacting subsonic edges. If the plan form has supersonic tips, however, the lower limit is the aspect ratio for which the trapezoid becomes a triangle.

The derivatives due to yawing were obtained from the application of the factor $\frac{\alpha(1-B^2)}{B^2}$ developed for the rectangular plan form. The justification of this step is given in a later section of the report wherein the sources and development of the results are discussed.

[2] In the terminology that has become associated with supersonic flow analysis, the term "subsonic edge" refers to an edge swept behind its Mach line (because the component of flow normal to the edge is subsonic) and the term "supersonic edge" refers to an edge swept ahead of its Mach line.

Triangular plan form with apex forward.—There is no aspect-ratio-parameter limitation necessary for the derivatives due to rolling or sideslip. The derivatives due to yawing, however, have been obtained only for plan forms having a BA of 4 or less because no solution, approximate or otherwise, has been developed for the yawing triangular wing with supersonic leading edges.

Triangular plan form with base forward.—For values of BA less than 4, the edges of this plan form become mutually interacting subsonic trailing edges and the reflections of the Mach lines establish an infinite number of regions which would have to be analyzed independently. This limit applies to the derivatives due to sideslip and yawing and would apply to the derivatives due to rolling if it were not for the fact that the reversability theorem (see reference 24) permits these derivatives to be calculated for the same plan-form range as obtained for the triangular plan forms with apex forward.

The derivatives due to yawing were obtained by applying the factor $\frac{\alpha(1-B^2)}{B^2}$ developed in the rectangular-wing analysis to the derivatives due to rolling. The justification of using this factor for a base-forward triangular plan form is given in a later section of this report. Inasmuch as the reversability theorem does not apply to the derivatives due to yawing, the lower limit for BA is 4 rather than zero.

Fully-tapered swept-back plan form.—The lower limit of BA, $4\frac{l}{c_r}\left(1-\frac{c_r}{l}\right)$, is common to all the derivatives in order to assure that the trailing edge of this plan form does not become subsonic. The upper limit of BA for the derivatives due to sideslip and yawing, $4l/c_r$, assures that the leading edge will not become supersonic. Values of the derivatives C_{l_p}, C_{n_p}, and C_{Y_p}, however, have been obtained from references 13 and 16 for plan forms having supersonic leading edges.

Swept-back hexagonal plan form.—The plan forms considered to fall in this classification have streamwise tips and range from the constant-chord swept-back, $\lambda=1$, to the swept-back plan form having a straight trailing edge, $A=4m(1-\lambda)/(1+\lambda)$. The aspect-ratio parameter range for this wing, given in table III, indicates that results are presented for plan forms having either subsonic or supersonic leading edges and having supersonic trailing edges. An added restriction provided by the limits on the aspect-ratio parameter range is that the Mach lines from the leading edges of the tips must not cross on the wing.

Unswept hexagonal plan form.—These plan forms have streamwise tips and range from the swept back with a straight trailing edge to the hexagonal plan form having fore-and-aft symmetry, which can be expressed as an aspect ratio range of

$$\frac{2m(1-\lambda)}{(1+\lambda)} \leq A \leq \frac{4m(1-\lambda)}{(1+\lambda)}$$

The results presented for the derivatives due to rolling and yawing are subject to the same aspect-ratio-parameter limitations that were given for the derivatives due to rolling for the swept-back hexagonal plan form.

Notched triangular plan form.—The derivatives due to rolling are presented for both subsonic and supersonic leading edges. It should be pointed out that for the damping-in-roll derivative the plan forms having subsonic leading edges differ from those having supersonic leading edges in that the trailing edges of the former always lie along the Mach line from the trailing end of the root chord; whereas the trailing edges of the latter are parallel to the leading edges. (See reference 2.) The derivatives due to sideslip are presented only for the plan form having supersonic leading edges.

SOURCES AND DEVELOPMENT OF RESULTS

The sources of the results for the lateral-stability derivatives of the various plan forms surveyed are listed in table I. An indication of the rigor which has been maintained in the individual developments of these results is given in the following discussion. Sources of some of the results available for plan forms other than those surveyed are also mentioned.

Derivative C_{l_p}: The rolling wing lends itself to readily specified boundary conditions and a rigorous application of the linearized-theory analysis. The damping moment obtained varies linearly with the rolling velocity p and, accordingly, the expression obtained for the derivative C_{l_p} is usually a relatively simple one. Furthermore, the numerical results are readily computed and can be presented in one figure showing both the variation with Mach number and aspect ratio. Consequently, there are more results available for the damping-in-roll derivative than for any of the other lateral derivatives, particularly in regard to the number of plan forms investigated.

In addition to the results presented in this summary, more extensive damping-in-roll results are available in the referenced reports for plan forms having arbitrary sweep and taper. In references 9 and 10, C_{l_p} is determined for such plan forms having subsonic leading edges and supersonic trailing edges. In reference 13, these results are extended to include such plan forms having supersonic leading and trailing edges. The effect of subsonic trailing edges has been investigated in references 11 and 15 using the cancellation-of-pressure technique, but the numerical results are limited to one or two plan forms. Values of C_{l_p} described as the upper limits for swept-back plan forms having subsonic trailing edges are presented in reference 9. These values were obtained by extending the expressions developed for C_{l_p} beyond the limits of applicability for which they were derived. The damping-in-roll derivative for swept-back tapered wings having raked-in or cross-stream tips and subsonic leading edges has been investigated and the results are presented in reference 12. Thus, it is possible to calculate the damping-in-roll derivative for a large number of plan forms of arbitrary sweep, taper, and tip rake. In some cases the numerical values of the derivative have been calculated and presented. In other cases the calculations must be carried out, a step which involves rather lengthy calculations when the trailing edges are subsonic and the cancellation techniques must be used.

It should be mentioned, however, that in many instances values for the damping-in-roll derivative can be determined

for plan forms and Mach angle configurations that would be extremely tedious if at all possible to calculate, by application of the plan form reversibility theorem presented in reference 24.

Derivative C_{n_p}: The contribution of the normal force to this derivative is $-\alpha C_{l_p}$ which can be evaluated from the damping-in-roll results previously discussed. The effects of edge suction on this derivative are also readily calculated. Thus it is possible to calculate C_{n_p} for the same extensive range of plan forms for which it was possible to calculate C_{l_p}. The results actually available for C_{n_p}, however, cover only the plan forms considered in this summary.

For the trapezoidal plan forms having raked-out tips, the expression for C_{n_p} applicable to the stability-axes system has not been published previously. For subsonic tips, and with the center of gravity located at $c_r/2$, the expression is,

$$C_{n_p}=\frac{-256\alpha\sqrt{1-B^2m^2}}{9\pi B^3A^3(1+Bm)\left(1+\sqrt{1-\frac{4Bm}{BA}}\right)^3}$$

$$\left\{B\left[\frac{3(1+Bm)(m^2-1)-2m^2}{\left(1+\sqrt{1-\frac{4Bm}{BA}}\right)}\right]-(BA)[3B(m^2-1)+m]+\right.$$

$$\frac{9B^2A^2}{8}m\left(1+\sqrt{1-\frac{4Bm}{BA}}\right)-$$

$$\left.\frac{B}{4}\left[9BA-\frac{12Bm}{\left(1+\sqrt{1-\frac{4Bm}{BA}}\right)}-\frac{8}{\left(1+\sqrt{1-\frac{4Bm}{BA}}\right)}\right]\right\}$$

and for supersonic tips the expression is

$$C_{n_p}=-\alpha C_{l_p}$$

Derivative C_{Y_p}: The derivative C_{Y_p} exists only when edge suction forces are present. The results available for C_{Y_p} cover only the plan forms considered in this summary and some swept-back tapered wings with streamwise tips having either supersonic or subsonic leading edges. (See references 14 and 16, respectively.)

The expressions for C_{Y_p} for the trapezoidal plan forms having raked-out or raked-in tips have not been published previously. For the subsonic raked-out-tip plan forms the expression applicable to the stability axes system is

$$C_{Y_p}=\frac{64\alpha\sqrt{1-B^2m^2}}{\pi B^2A^2(1+Bm)\left(1+\sqrt{1-\frac{4Bm}{BA}}\right)^2}$$

$$\left[BA-\frac{4Bm}{3\left(1+\sqrt{1-\frac{4Bm}{BA}}\right)}-\frac{8}{9\left(1+\sqrt{1-\frac{4Bm}{BA}}\right)}\right]$$

For the supersonic raked-out-tip plan forms and for the raked-in-tip plan forms there is no suction effect and C_{Y_p} is, consequently, zero.

Derivative C_{l_β}: For wings in sideslip, the boundary conditions are easily specified and the linearized-theory analysis to obtain the normal force is easily carried out. Unfortunately, however, the rolling moment cannot be generally expressed as a linear function of sideslip angle. (See reference 5.) To obtain the derivative C_{l_β}, therefore, it is necessary to plot C_l against the sideslip angle β and to measure the slope or, if the sideslip is restricted to very small angles (reference 4), it is possible to linearize the expression for C_l and obtain an explicit expression for C_{l_β}. Although no derivatives due to sideslip are presented for the unswept and swept-back hexagonal plan forms, these derivatives can be calculated for these plan forms using references 21, 22, or 23, or if a cancellation technique is needed, reference 18 gives a demonstration that is directly applicable to these cases.

It should be pointed out that for the trapezoidal plan forms with a tip slope m of $\pm\frac{1}{2}$ the Mach cones and tips coincide at $B=2$. Double values of the derivatives due to sideslip, C_{l_β}, C_{n_β}, and C_{Y_β}, occur at this value of B and in order to avoid any ambiguity the limiting values of the derivatives obtained by approaching $B=2$ from the lower values of B (tips subsonic) were labeled $B=2$ (−) and the limiting values of the derivatives obtained by approaching from higher values of B (tips supersonic) were labeled $B=2$ (+).

For plan forms having streamwise tips, such as rectangular plan forms, there is some doubt as to the validity of the results obtained by applying the Kutta condition to the trailing tip at small angles of sideslip. In reference 6 it is assumed that the Kutta condition does not apply, whereas in reference 5 it is assumed that the Kutta condition applies to the trailing tip at small angles of sideslip as well as large. This difference in basic assumptions leads to two entirely different values for C_{l_β}. From physical considerations of what the flow must be past a sharp trailing edge, such as the tip of a thin airfoil, the theoretical analysis based on the latter assumption is the correct one. From physical considerations of the flow about a wing tip of finite thickness, the correctness of either assumption depends upon the ability of the boundary layer on the tip to resist separation. If the suction force caused by the high velocity flow of air from the bottom surface to the top surface is strong enough to cause the boundary layer to separate, then a flow corresponding to the Kutta condition will result and the edge suction force will no longer exist. The angle of sideslip at which separation of the flow around the tip will take place is, at present, undetermined. It will depend on the angle of attack and on the shape of the tip to a large extent. It is definitely possible, however, for separation to occur on tips raked at a slight angle into the stream, such as the advancing tip of the rectangular wing in sideslip, as well as on a trailing tip. If this were the case, the Kutta condition would have to be applied to both tips at small angles of sideslip rather than to one or neither as assumed in the previously mentioned analyses. Until experimental results are obtained that will provide definite quantitative evidence to the contrary, therefore, it seems most reasonable to assume that the solution based on the flow over a thin trailing edge is valid. In other words, it seems most reasonable to assume that the Kutta condition holds for all trailing edges and the edge suction exists on all leading edges no matter what the angle of inclination is

between the edge and the stream. Accordingly, the results presented in this survey correspond to those reported in reference 5.

Derivative C_{n_β}: The contribution of the edge suction effects to this derivative is easily estimated but the resulting expression for the yawing moment is nonlinear with sideslip. The normal force contribution $-\alpha C_{l_\beta}$ is also nonlinear with sideslip as described in the discussion of C_{l_β}. Both of these nonlinearities can be handled, however, in the manner mentioned in that discussion.

For the plan forms having streamwise tips the application of the Kutta condition to the trailing tip at small angles of sideslip causes a jump in the yawing-moment curve at zero sideslip. (See references 8 and 17.) This jump makes it difficult to establish a rational value for C_{n_β} especially in view of the fact that in actuality the jump will, undoubtedly, be rounded off and the curve will have no discontinuity in slope at zero sideslip. The value of the derivative selected for the curve with the jump was based on the slope of the yawing-moment curve as it approached zero sideslip. This value is questionable in magnitude. It has the proper sign, however, and should be an underestimation of the actual value of C_{n_β}.

Derivative C_{Y_β}: Inasmuch as the edge-suction force is the only source of side force for wing plan forms, the derivative C_{Y_β} is zero (at zero sideslip) for plan forms having supersonic raked-out tips or raked-in tips. For trapezoidal plan forms having subsonic tips, the expression for the side force is

$$C_{Y_\beta}=\frac{-32\alpha^2}{\pi A\left(1+\sqrt{1-\frac{4Bm}{BA}}\right)^2}\frac{(1+B^2)}{B^2(1+Bm)\sqrt{1-B^2m^2}}$$

The jump that appears in the yawing moment versus sideslip curve at zero sideslip for plan forms having streamwise tips occurs also in the side force versus sideslip curve. The evaluation of the derivatives under these conditions was handled in the manner described in the discussion of C_{n_β}.

Derivative C_{l_r}: As mentioned in a preceding section of this report, the yawing wing cannot be fitted satisfactorily to quasi-steady boundary conditions that would permit the use of an exact linearized-theory analysis based on a steady-state flow. For rectangular and triangular wings, however, modified strip-theory analyses have been applied in references 6 and 4, respectively, and approximate values for the rolling-moment-due-to-yawing derivative have been obtained. The analysis for the triangular wing takes into account the spanwise variation of speed but not the spanwise variation of Mach number. A chordwise variation of the effective sideslip angle for a yawing wing is also included in the triangular-wing analysis. The contribution of this latter factor is predominant for triangular wings of low aspect ratio (that is, triangular wings having small vertex angles). Both the spanwise variations of Mach number and of speed were taken into account in a somewhat similar analysis for the rectangular wing. From this latter analysis a factor of $\frac{\alpha(1-B^2)}{B^2}$ was found to exist between the loading due to rolling and the loading due to yawing over the portion of the rectangular wing where the flow was two dimensional, and it was assumed that this factor could also be applied in the vicinity of the tips. An analysis of a rectangular wing of infinite span based on unsteady flow, made in reference 20, provided verification of the existence of the factor $\frac{\alpha(1-B^2)}{B^2}$ for the region of two-dimensional flow. In view of this verification, it seems that the rectangular-wing values for C_{l_r} obtained from reference 6 should be a good approximation, at least for plan forms having high aspect ratios. Furthermore, application of the factor $\frac{\alpha(1-B^2)}{B^2}$ to the rolling-moment results for a trapezoidal plan form having supersonic raked-in tips should provide exact theoretical values for C_{l_r} (using the unsteady-flow-analysis results as a norm) because of the lack of tip effects. Inasmuch as any plan form having relatively large regions of two-dimensional flow should be suited to this approximate analysis, it was decided to use this factor to obtain approximate values of C_{l_r} for the trapezoidal plan forms, the base-forward triangular plan form with supersonic tips, and the unswept hexagonal plan form. By this step, theoretical estimates of C_{l_r} were made available for all but the apex-forward triangular plan form with supersonic leading edges, the base-forward triangular plan form with subsonic trailing edges, the swept-back hexagonal plan form, and the notched triangular plan form.

Derivative C_{n_r}: Application of the factor $\frac{\alpha(1-B^2)}{B^2}$ to the calculation of the edge-suction-force contribution to C_{n_r} from the edge-suction force due to rolling will yield an admittedly rougher approximation than the application of this factor to the determination of the normal force due to yawing. However, in view of the fact that it was the only method available for estimating the edge-suction force in yawing, it was used to obtain the C_{n_r} results for all the plan forms similarly analyzed for C_{l_r}.

Derivative C_{Y_r}: The application of the factor $\frac{\alpha(1-B^2)}{B^2}$ to calculate C_{l_r} and C_{n_r} from C_{l_p} and C_{n_p}, respectively, for certain plan forms was extended to the side-force calculations in order to obtain values for the derivative C_{Y_r}. The apex-forward triangular plan form having subsonic leading edges was excepted inasmuch as the derivative C_{Y_r} was available from reference 4.

CONCLUDING REMARKS

Values of the lateral-stability derivatives for wings at supersonic speeds, calculated using the linearized theory for compressible flow, have been presented in the form of design charts showing the variations of the derivatives with Mach number and aspect ratio for nine plan forms. These plan forms were: (1) rectangular; (2) trapezoidal with raked-out tips; (3) trapezoidal with raked-in tips; (4) triangular with apex forward; (5) triangular with base forward; (6) fully

tapered swept-back; (7) swept-back hexagonal; (8) unswept hexagonal; and (9) notched triangular.

Limitations in the applicability and availability of the lateral-stability derivatives are discussed.

AMES AERONAUTICAL LABORATORY,
NATIONAL ADVISORY COMMITTEE FOR AERONAUTICS,
MOFFETT FIELD, CALIF., *June 26, 1951.*

REFERENCES

1. Ribner, Herbert S.: The Stability Derivatives of Low-Aspect-Ratio Triangular Wings at Subsonic and Supersonic Speeds. NACA TN 1423, 1947.
2. Jones, Arthur L., and Alksne, Alberta: The Damping Due to Roll of Triangular, Trapezoidal, and Related Plan Forms in Supersonic Flow. NACA TN 1548, 1948.
3. Brown, Clinton E., and Adams, Mac C.: Damping in Pitch and Roll of Triangular Wings at Supersonic Speeds. NACA Rep. 892, 1948.
4. Ribner, Herbert S., and Malvestuto, Frank S., Jr.: Stability Derivatives of Triangular Wings at Supersonic Speeds. NACA Rep. 908, 1948. (Formerly NACA TN 1572)
5. Jones, Arthur L., Spreiter, John R., and Alksne, Alberta: The Rolling Moment Due to Sideslip of Triangular, Trapezoidal, and Related Plan Forms in Supersonic Flow. NACA TN 1700, 1948.
6. Harmon, Sidney M.: Stability Derivatives at Supersonic Speeds of Thin Rectangular Wings with Diagonals Ahead of Tip Mach Lines. NACA Rep. 925, 1949. (Formerly NACA TN 1706)
7. Malvestuto, Frank S., Jr., and Margolis, Kenneth: Theoretical Stability Derivatives of Thin Sweptback Wings Tapered to a Point with Sweptback and Sweptforward Trailing Edges for a Limited Range of Supersonic Speeds. NACA TN 1761, 1949.
8. Jones, Arthur L., and Alksne, Alberta: The Yawing Moment Due to Sideslip of Triangular, Trapezoidal, and Related Plan Forms in Supersonic Flow. NACA TN 1850, 1949.
9. Malvestuto, Frank S., Jr., Margolis, Kenneth, and Ribner, Herbert S.: Theoretical Lift and Damping in Roll of Thin Sweptback Wings of Arbitrary Taper and Sweep at Supersonic Speeds. Subsonic Leading Edges and Supersonic Trailing Edges. NACA TN 1860, 1949.
10. Piland, Robert O.: Summary of the Theoretical Lift, Damping-in-Roll, and Center-of-Pressure Characteristics of Various Wing Plan Forms at Supersonic Speeds. NACA TN 1977, 1949.
11. Walker, Harold J., and Ballantyne, Mary B.: Pressure Distribution and Damping in Steady Roll at Supersonic Mach Numbers of Flat Swept-Back Wings with Subsonic Edges. NACA TN 2047, 1950.
12. Margolis, Kenneth: Theoretical Lift and Damping in Roll of Thin Sweptback Tapered Wings with Raked-In and Cross-Stream Wing Tips at Supersonic Speeds. Subsonic Leading Edges. NACA TN 2048, 1950.
13. Harmon, Sidney M., and Jeffreys, Isabella: Theoretical Lift and Damping in Roll of Thin Wings with Arbitrary Sweep and Taper at Supersonic Speeds. Supersonic Leading and Trailing Edges. NACA TN 2114, 1950.
14. Margolis, Kenneth: Theoretical Calculations of the Lateral Force and Yawing Moment Due to Rolling at Supersonic Speeds for Sweptback Tapered Wings with Streamwise Tips. Subsonic Leading Edges. NACA TN 2122, 1950.
15. Ribner, Herbert S.: On the Effect of Subsonic Trailing Edges on Damping in Roll and Pitch of Thin Sweptback Wings in a Supersonic Stream. NACA TN 2146, 1950.
16. Harmon, Sidney M., and Martin, John C.: Theoretical Calculations of the Lateral Force and Yawing Moment Due to Rolling at Supersonic Speeds for Sweptback Tapered Wings with Streamwise Tips. Supersonic Leading Edges. NACA TN 2156, 1950.
17. Jones, Arthur L.: The Theoretical Lateral-Stability Derivatives for Wings at Supersonic Speeds. Jour. Aero. Sci., vol. 17, no. 1, Jan. 1950, pp. 39–46.
18. Lampert, Seymour: Rolling and Yawing Moments for Swept-Back Wings in Sideslip at Supersonic Speeds. NACA TN 2262, 1951.
19. Glauert, H.: A Non-Dimensional Form of the Stability Equations of an Aeroplane. British A. R. C., R. & M. 1093, 1927.
20. Lomax, Harvard, Heaslet, Max. A., and Fuller, Franklyn B.: Three-Dimensional, Unsteady-Lift Problems in High-Speed Flight—Basic Concepts. NACA TN 2256, 1950.
21. Heaslet, Max. A., and Lomax, Harvard: The Use of Source-Sink and Doublet Distributions Extended to the Solution of Arbitrary Boundary Value Problems in Supersonic Flow. NACA Rep. 900, 1948. (Formerly NACA TN 1515)
22. Evvard, John C.: Theoretical Distribution of Lift on Thin Wings at Supersonic Speeds (an Extension). NACA TN 1585, 1948.
23. Pell, William H.: Lifting Surfaces in Supersonic Flow. Part II—Linearized Three-Dimensional Theory. AMC Technical Report 102-AC49/8-100, December 1949.
24. Brown, Clinton E.: The Reversability Theorem for Thin Airfoils in Subsonic and Supersonic Flow. NACA TN 1944, 1949.

TABLE I.—REFERENCE NUMBERS OF THE SOURCES OF THE STABILITY—DERIVATIVE RESULTS SUMMARIZED

Derivative \ Plan form	Rectangular	Trapezoidal with raked-out tips	Trapezoidal with raked-in tips	Triangular with apex forward	Triangular with base forward	Swept back	Swept-back hexagonal	Unswept hexagonal	Notched triangular
C_{l_p}	2, 6	2	2	2, 4	2, 4	7, 9	9, 10, 11, 13, 15	9, 10, 11, 13, 15	2
C_{n_p}	6	(1)	2	4	2, 4	7, 14, 16	14, 16	14, 16	------
C_{Y_p}	6	(1)	(1)	4	(1)	7, 14, 16	14, 16	14, 16	------
C_{l_β}	5, 6	5	5	4, 5	5	5, 7	----------	----------	5
C_{n_β}	6, 8	8	8	4, 8	8	7, 8	----------	----------	8
C_{Y_β}	6	(1)	(1)	4	(1)	7	----------	----------	(1)
C_{l_r}	6	[2] 6	[2] 6	4	[2] 6	7	----------	[2] 6	------
C_{n_r}	6	[2] 6	[2] 6	4	[2] 6	7	----------	[2] 6	------
C_{Y_r}	6	[2] 6	[2] 6	4	[2] 6	7	----------	[2] 6	------

[1] Previously unpublished. [2] By extension.

TABLE II.—FIGURE NUMBERS FOR DERIVATIVES AND PLAN FORMS [1]

Derivative \ Plan form	Rectangular	Trapezoidal with raked-out tips	Trapezoidal with raked-in tips	Triangular with apex forward	Triangular with base forward	Swept back	Swept-back hexagonal	Unswept hexagonal	Notched triangular
C_{l_p}	3(a)	3(a), 4, 20	3(a), 4, 20	3(a)	3(a)	3(a), 29	3(b), 3(c), 3(d), 38, 41, 59, 56	3(e), 44, 3(f), 50, 62	3(g)
C_{n_p}	5(a), 6(a)	5(b), 6(b), 21	5(c), 6(c), 21	5(d), 6(d)	5(e), 6(e)	5(f), 6(f), 30	5(g), 5(h), 5(i), 6(g), 6(h), 6(i), 39, 42, 57, 60	5(j), 6(j), 5(k), 6(k), 45, 51, 63	------
C_{Y_p}	7(a)	7(a), 22	7(a), 22	7(a)	7(a)	7(a), 31	7(b), 7(c), 40, 43, 58, 61	7(d), 7(e), 46, 52, 64	------
C_{l_β}	8(a), 9(a)	8(b), 9(b), 23	8(c), 9(c), 23	8(d), 9(d)	8(e), 9(e)	8(f), 9(f), 32	----------	----------	8(g)
C_{n_β}	10(a), 11(a)	10(b), 11(b), 24	10(c), 11(c), 24	10(d), 11(d)	10(e), 11(e)	10(f), 11(f), 33	----------	----------	10(g), 11(g)
C_{Y_β}	12(a), 13(a)	12(b), 13(b), 25	12(c), 13(c), 25	12(d), 13(d)	12(e), 13(e)	12(f), 13(f), 34	----------	----------	12(g), 13(g)
C_{l_r}	14(a), 15(a)	14(b), 15(b), 26	14(c), 15(c), 26	14(d), 15(d)	14(e), 15(e)	14(f), 15(f), 35	----------	14(g), 15(g), 14(h), 15(h), 47, 53, 65	------
C_{n_r}	16(a), 17(a)	16(b), 17(b), 27	16(c), 17(c), 27	16(d), 17(d)	16(e), 17(e)	16(f), 17(f), 36	----------	16(g), 17(g), 16(h), 17(h), 48, 54, 66	------
C_{Y_r}	18(a), 19(a)	18(b), 19(b), 28	18(c), 19(c), 28	18(d), 19(d)	18(e), 19(e)	18(f), 19(f), 37	----------	18(g), 19(g), 18(h), 19(h), 49, 55, 67	------

[1] In cases where more than one curve falls on a single line, the leaders identifying the curves are used to indicate the lower limit of each curve with respect to the variable plotted horizontally.

TABLE III.—RANGES OF ASPECT-RATIO PARAMETER FOR WHICH DERIVATES ARE PRESENTED

Derivative \ Plan form	Rectangular	Trapezoidal [1] with raked-out tips	Trapezoidal [1] with raked-in tips	Triangular with apex forward	Triangular with base forward
C_{l_p}	$1 \leq BA \leq \infty$	$(1+Bm)^2 \leq BA \leq \infty$	$(1-Bm)^2 \leq BA \leq \infty$	$0 \leq BA \leq \infty$	$0 \leq BA \leq \infty$
C_{n_p}	----do----	----do----	----do----	----do----	Do.
C_{Y_p}	----do----	----do----	----do----	----do----	Do.
C_{l_β}	----do----	----do----	----do----	----do----	$4 \leq BA \leq \infty$
C_{n_β}	----do----	----do----	----do----	----do----	Do.
C_{Y_β}	----do----	----do----	----do----	----do----	Do.
C_{l_r}	----do----	----do----	----do----	$0 \leq BA \leq 4$	Do.
C_{n_r}	----do----	----do----	----do----	----do----	Do.
C_{Y_r}	----do----	----do----	----do----	----do----	Do.

[1] Limits given are for subsonic tips ($|Bm|<1$); for supersonic tips ($|Bm|\geq 1$) the limits are $|4Bm| \leq BA \leq \infty$.

TABLE III.—CONCLUDED

Derivative \ Plan form	Swept back	Swept-back [2] hexagonal	Unswept [2] hexagonal	Notched triangular
C_{l_p}	$\frac{4l}{c_r}\left(1-\frac{c_r}{l}\right) \leq BA \leq \infty$	$\frac{4Bm}{(Bm+1)(1+\lambda)} \leq BA \leq \frac{4Bm(1-\lambda)}{(1-Bm)(1+\lambda)}$	$\frac{4Bm}{(Bm+1)(1+\lambda)} \leq BA \leq \frac{4Bm(1-\lambda)}{(1-Bm)(1+\lambda)}$	$0 \leq BA \leq \frac{4l}{c_r\left(2-\frac{c_r}{l}\right)\left(1-\frac{c_r}{l}\right)}$
C_{n_p}	-----do-----	-----do-----	-----do-----	----------
C_{Y_p}	-----do-----	-----do-----	-----do-----	----------
C_{l_β}	$\frac{4l}{c_r}\left(1-\frac{c_r}{l}\right) \leq BA \leq \frac{4l}{c_r}$	----------	----------	$\frac{4l}{c_r\left(2-\frac{c_r}{l}\right)} \leq BA \leq \frac{4l}{c_r\left(2-\frac{c_r}{l}\right)\left(1-\frac{c_r}{l}\right)}$
C_{n_β}	-----do-----	----------	----------	Do.
C_{Y_β}	-----do-----	----------	----------	Do.
C_{l_r}	-----do-----	----------	$\frac{4Bm}{(Bm+1)(1+\lambda)} \leq BA \leq \frac{4Bm(1-\lambda)}{(1-Bm)(1+\lambda)}$	----------
C_{n_r}	-----do-----	----------	-----do-----	----------
C_{Y_r}	-----do-----	----------	-----do-----	----------

[2] These limits apply for subsonic leading edges, $Bm<1$, but for supersonic leading edges, $Bm\geq 1$, the upper limit is changed to ∞.

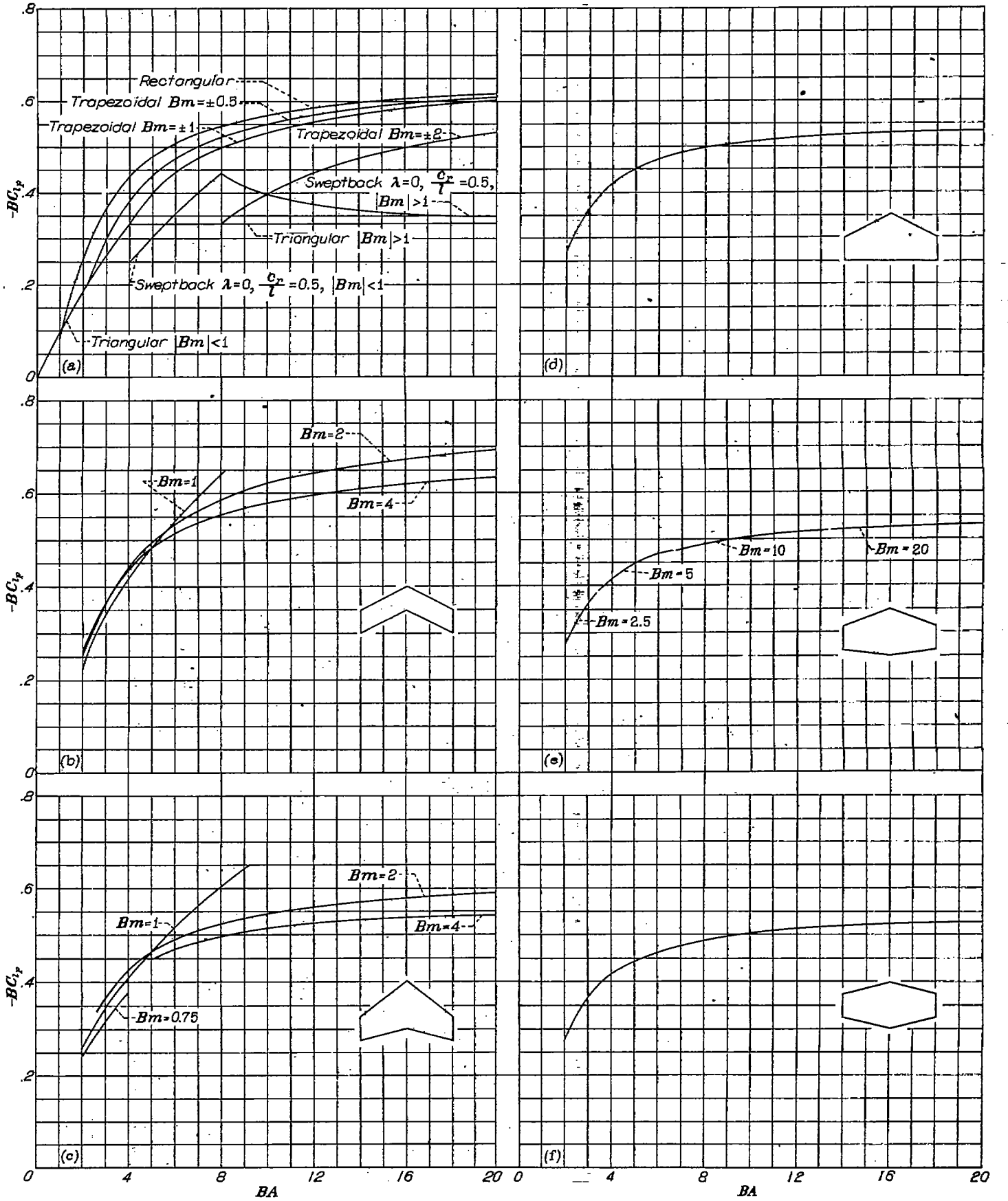

(a) First six plan forms investigated.

(b) Swept-back hexagonal plan form; λ=1.

(c) Swept-back hexagonal plan form; λ=0.5.

(d) Swept-back hexagonal plan form; λ=0.5, $Bm=3B_{1/4}$.

(e) Unswept hexagonal plan form; λ=0.5.

(f) Unswept hexagonal plan form; λ=0.5; $Bm=3BA/2$.

FIGURE 3.—Variation of damping-in-roll parameter with aspect-ratio parameter.

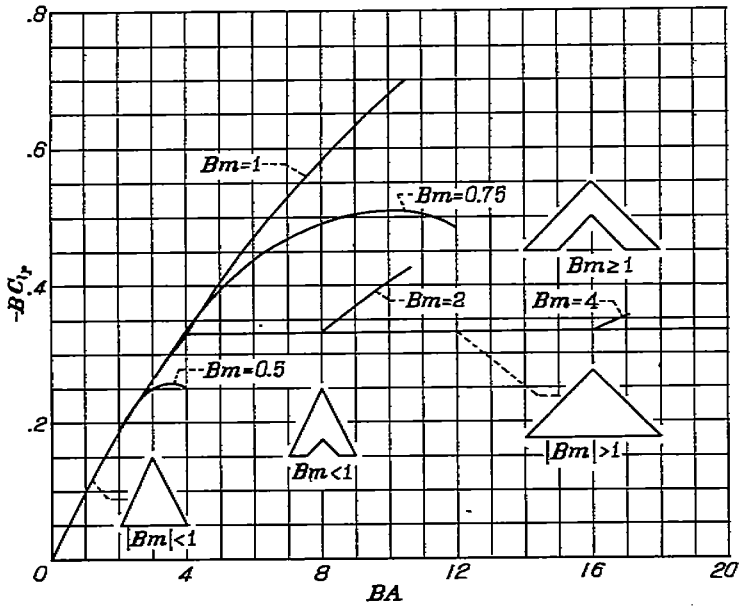

FIGURE 3.—Concluded. (g) Triangular and notched triangular plan forms.

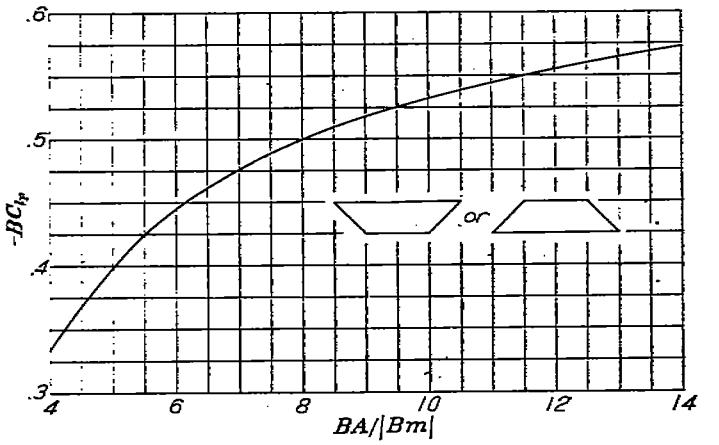

FIGURE 4.—Variation of damping-in-roll parameter with plan-form parameter for trapezoidal plan forms having supersonic tips; $|Bm| \geq 1$.

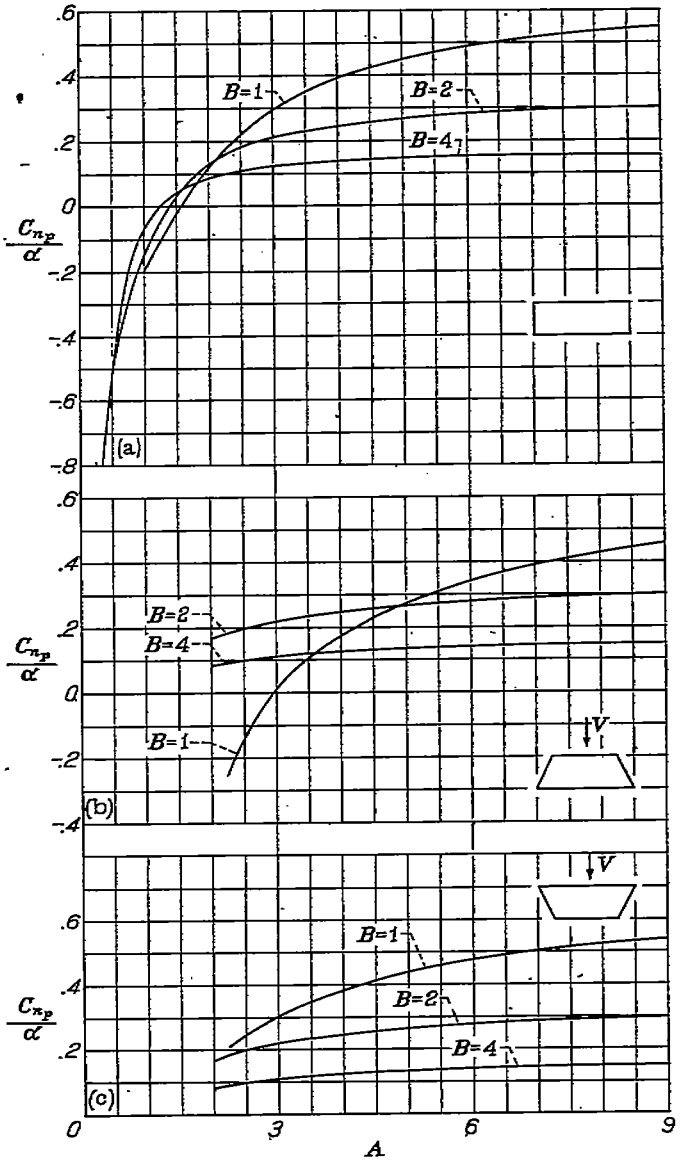

(a) Rectangular plan form.

(b) Trapezoidal plan form; $m=0.5$.

(c) Trapezoidal plan form; $m=-0.5$.

FIGURE 5.—Variation of yawing-moment-due-to-roll derivative with aspect ratio.

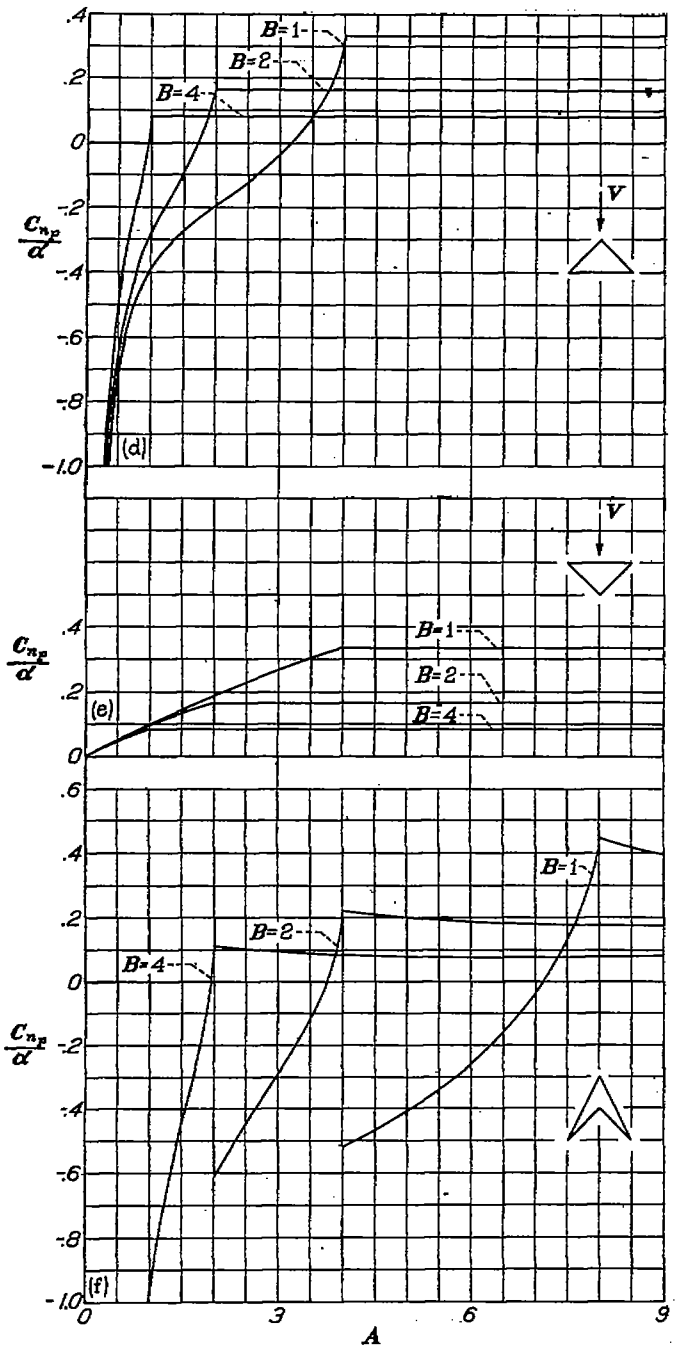

(d) Triangular plan form. Apex forward.

(e) Triangular plan form. Base forward.

(f) Swept-back plan form; $\lambda=0$; $\frac{c_r}{l}=0.5$.

FIGURE 5.—Continued.

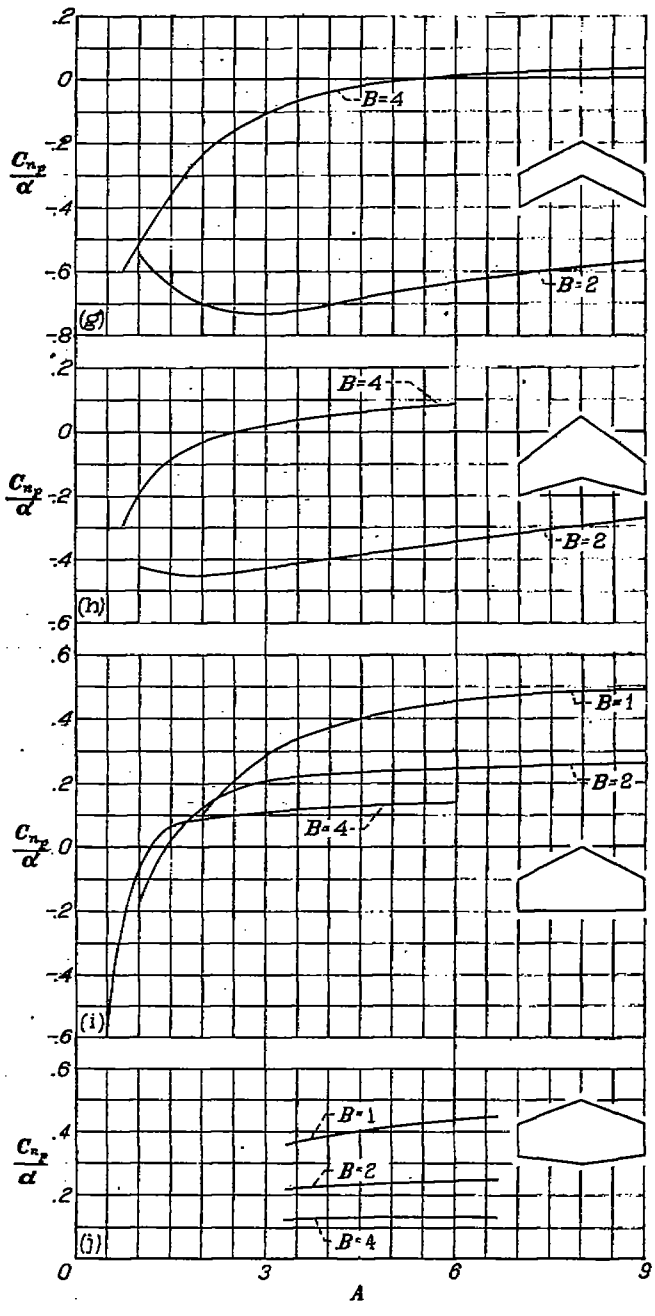

(g) Swept-back hexagonal plan form; $\lambda=1.0$; $m=0.5$.

(h) Swept-back hexagonal plan form; $\lambda=0.5$; $m=0.5$.

(i) Swept-back hexagonal plan-form; $\lambda=0.5$, $Bm=3BA/4$.

(j) Unswept hexagonal plan form; $\lambda=0.5$; $m=5$

FIGURE 5.—Continued.

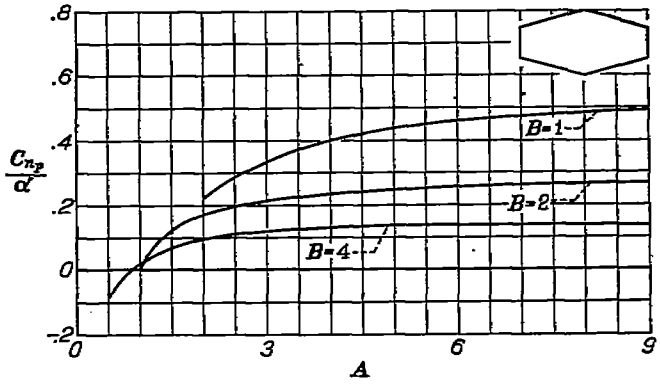

FIGURE 5.—Concluded. (k) Unswept hexagonal plan form; $\lambda=0.5$; $Bm=3BA/2$.

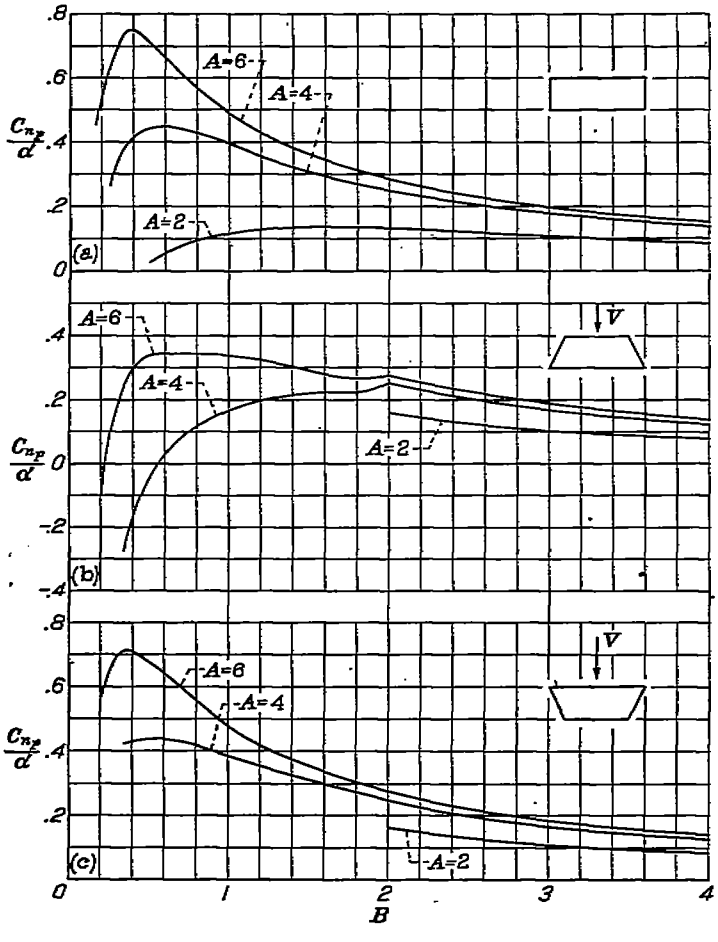

(a) Rectangular plan form.

(b) Trapezoidal plan form; $m=0.5$.

(c) Trapezoidal plan form; $m=-0.5$.

FIGURE 6.—Variation of yawing-moment-due-to-roll derivative with Mach number parameter B.

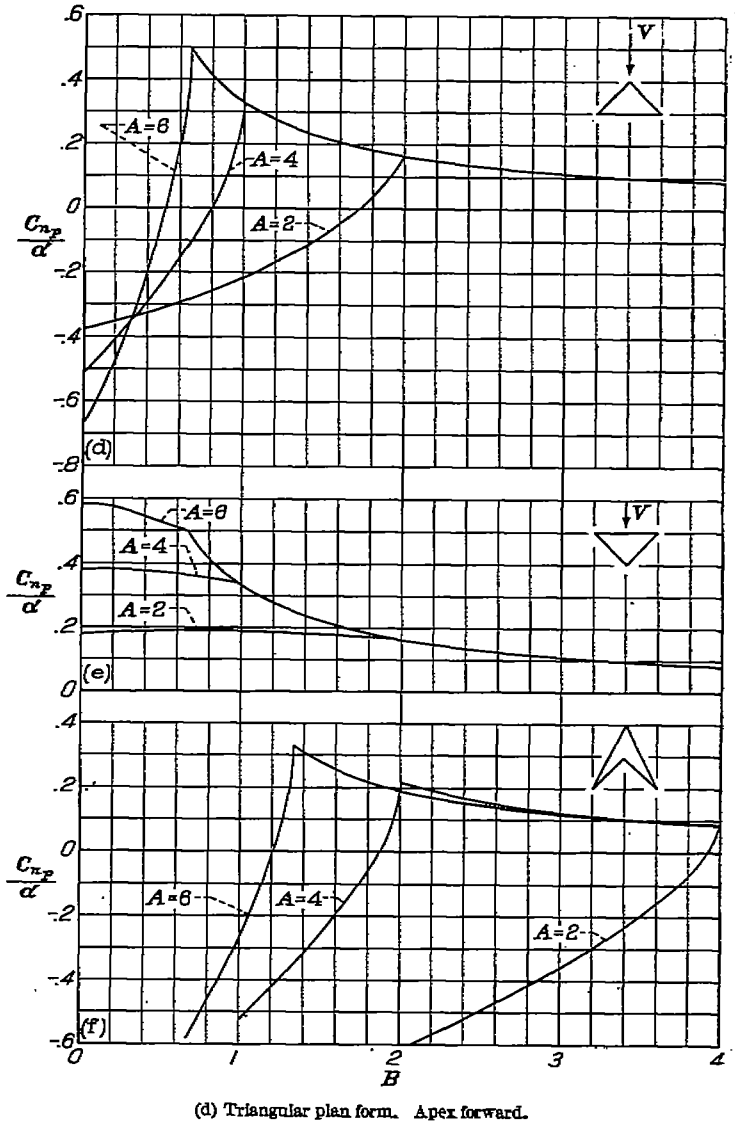

(d) Triangular plan form. Apex forward.

(e) Triangular plan form. Base forward.

(f) Swept-back plan form; $\lambda=0$; $\frac{c_r}{l}=0.5$.

FIGURE 6.—Continued.

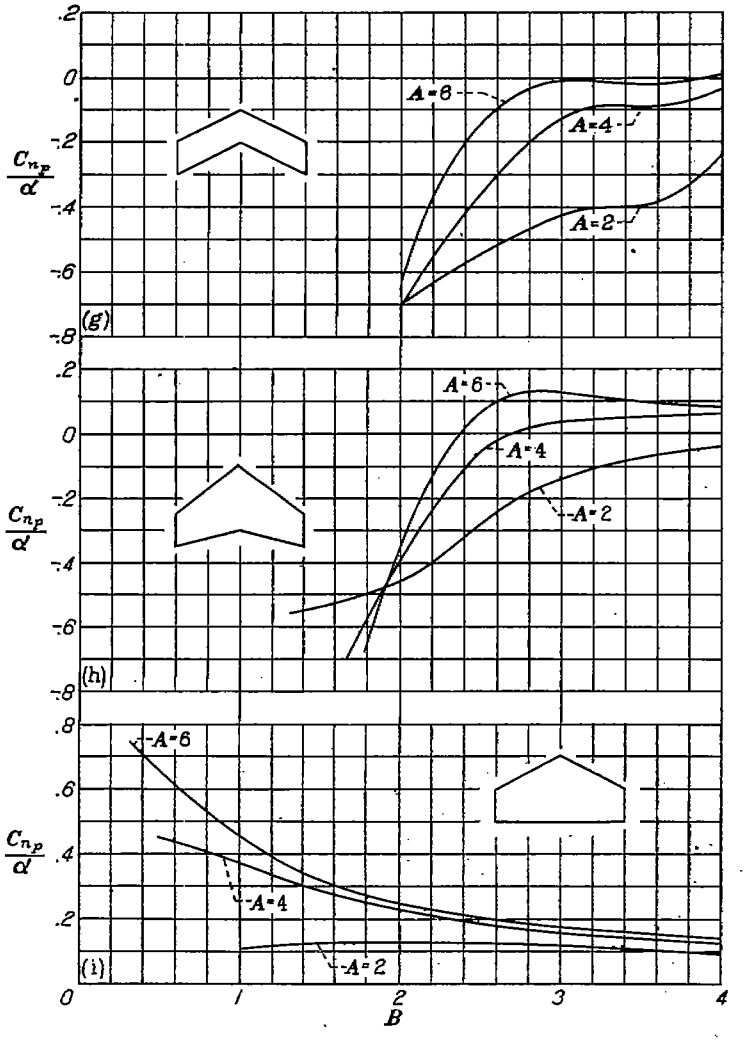

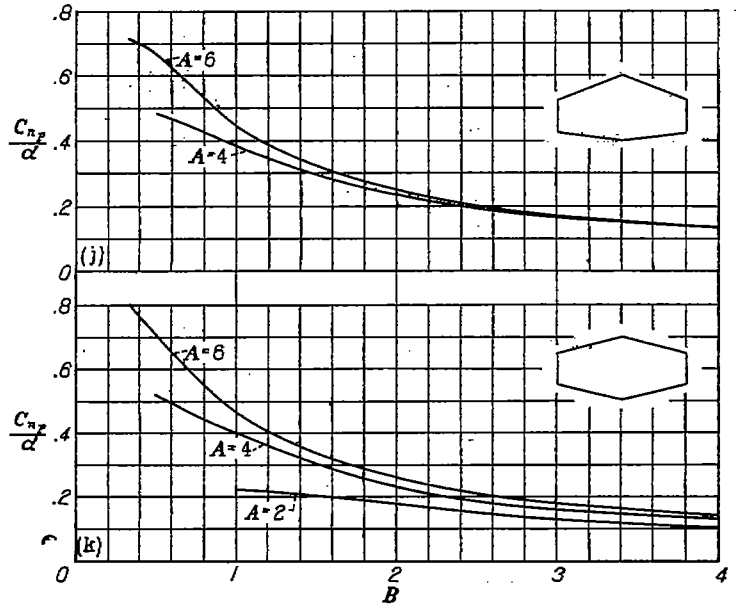

(g) Swept-back hexagonal plan form; λ=1.0; m=0.5.

(h) Swept-back hexagonal plan form; λ=0.5; m=0.5.

(i) Swept-back hexagonal form; λ=0.5, Bm=3B.4/4.

(j) Unswept hexagonal plan form; λ=0.5; m=5.

(k) Unswept hexagonal plan form; λ=0..5; Bm=3B.4/2.

FIGURE 6.—Concluded.

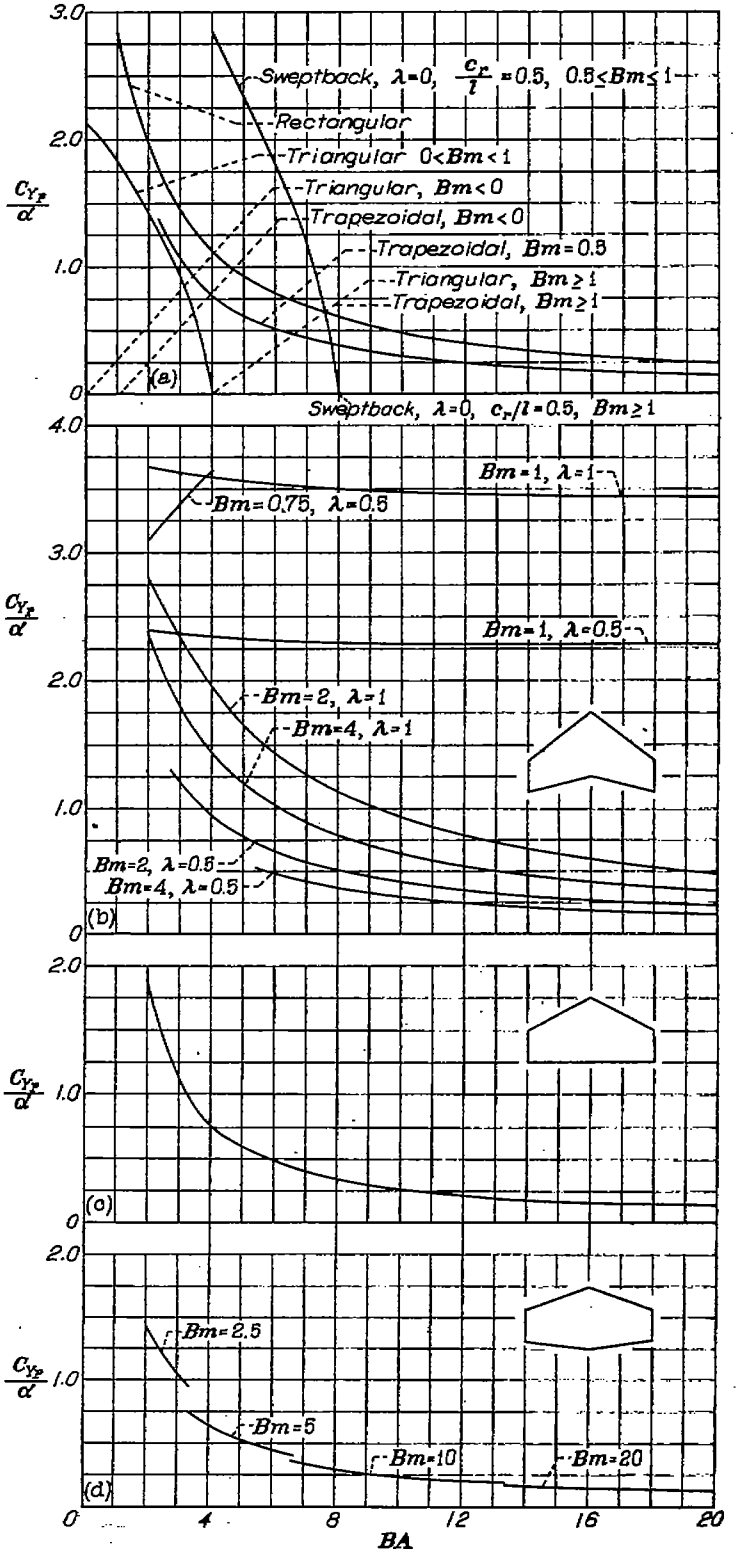

(a) First six plan forms investigated. (See footnote, table II.)

(b) Swept-back hexagonal plan form.

(c) Swept-back hexagonal plan form; λ=0.5. Bm=3B.4/4.

(d) Unswept hexagonal plan form; λ=0.5.

FIGURE 7.—Variation of side-force-due-to-rolling derivative with aspect-ratio parameter.

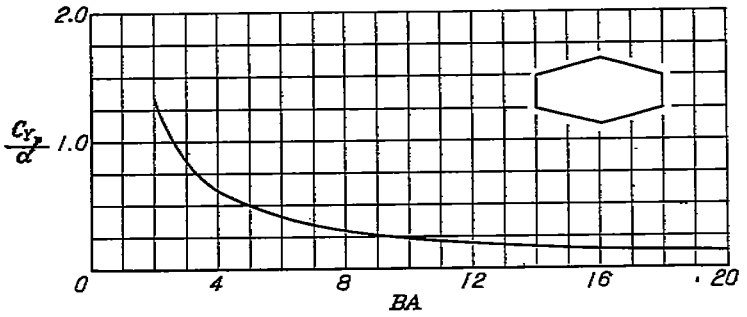

FIGURE 7.—Concluded. (e) Unswept hexagonal plan form; $\lambda=0.5$; $Bm=8BA/2$.

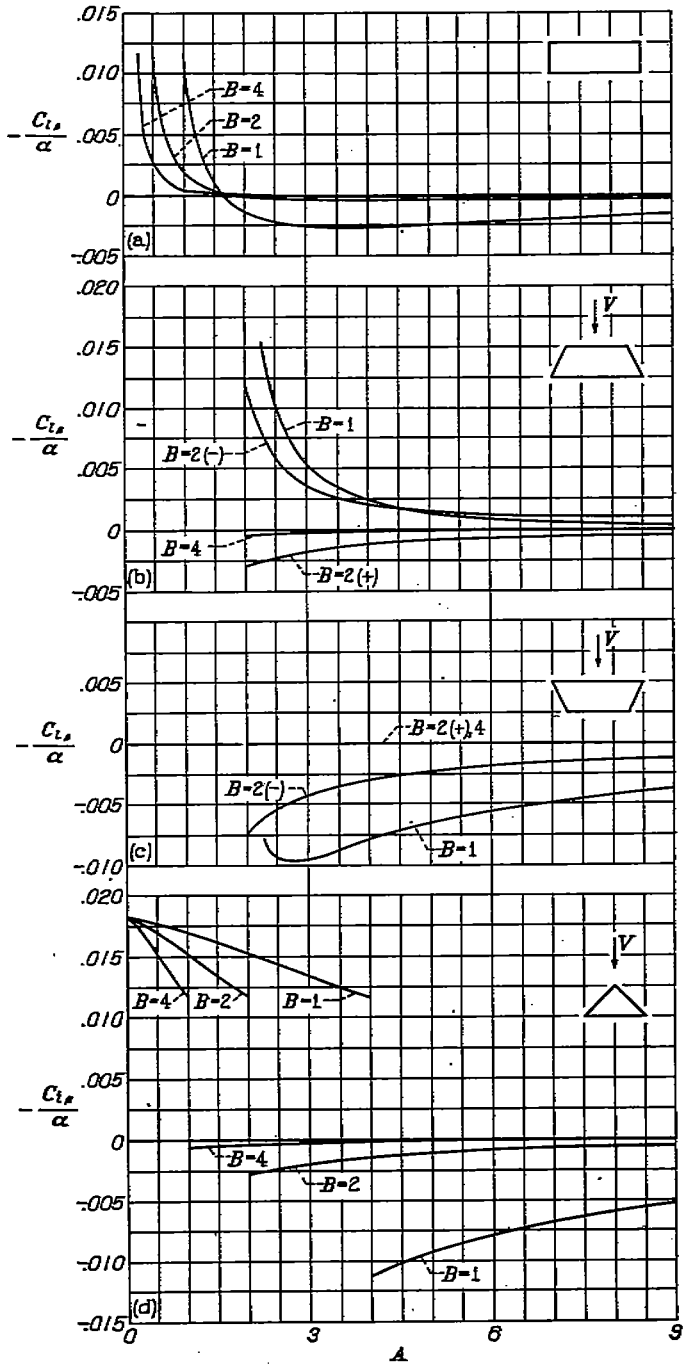

(a) Rectangular plan form.

(b) Trapezoidal plan form; $m=0.5$.

(c) Trapezoidal plan form; $m=-0.5$.

(d) Triangular plan form. Apex forward.

FIGURE 8.—Variation of rolling-moment-due-to-sideslip derivative with aspect ratio.

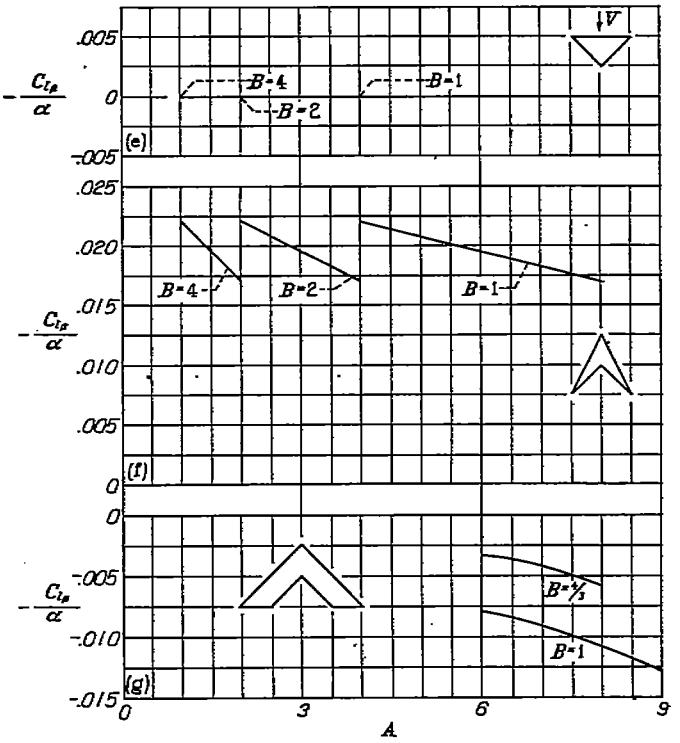

(e) Triangular plan form. Base forward. (See footnote, table II.)

(f) Swept-back plan form; $\lambda=0$; $\frac{c_r}{l}=0.5$.

(g) Notched triangular plan form; $m=\frac{3}{4}$.

FIGURE 8.—Concluded.

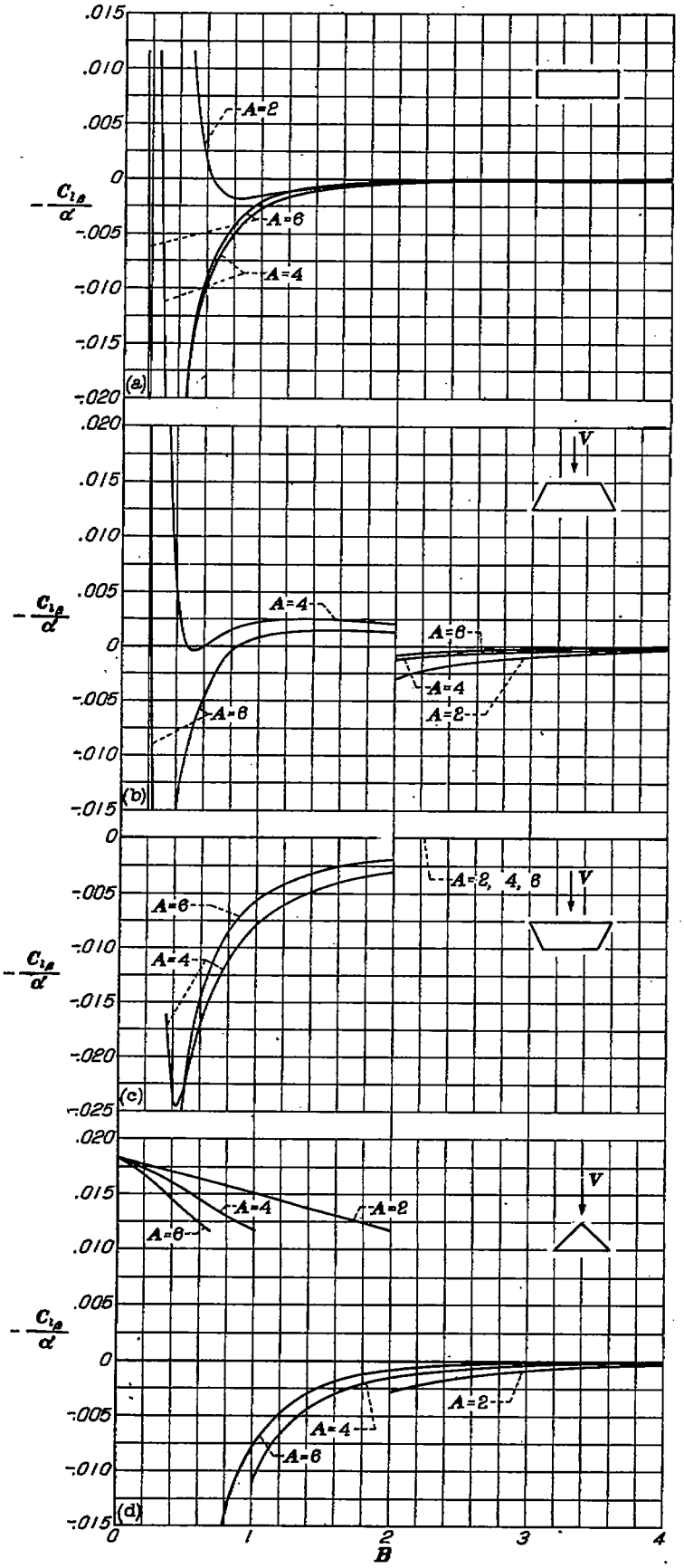

(a) Rectangular plan form.

(b) Trapezoidal plan form; $m=0.5$.

(c) Trapezoidal plan form; $m=-0.5$.

(d) Triangular plan form. Apex forward.

FIGURE 9.—Variation of rolling-moment-due-to-sideslip derivative with Mach number parameter B.

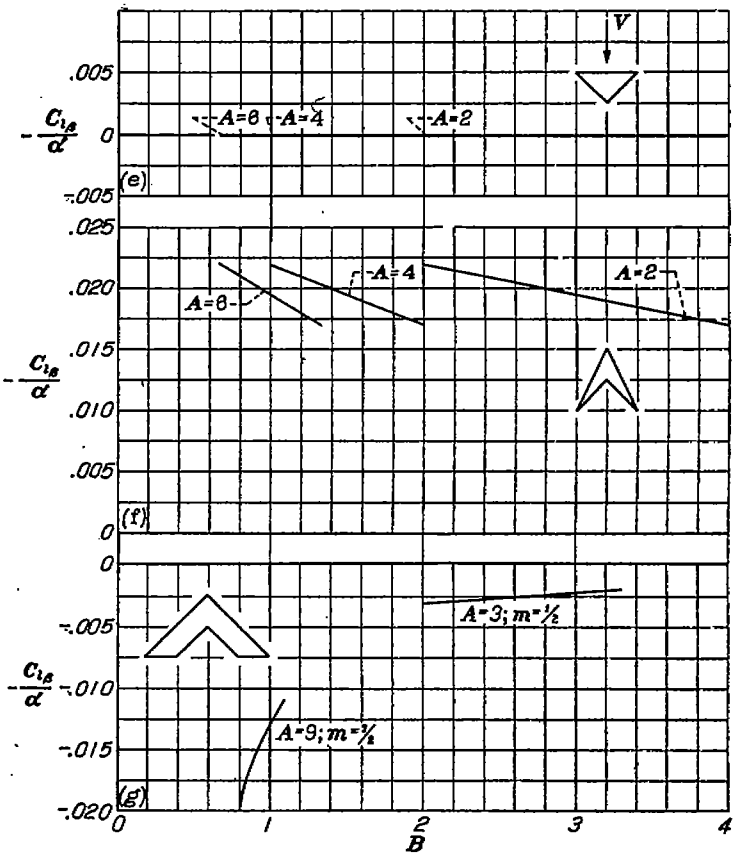

(e) Triangular plan form. Base forward. (See footnote, table II.

(f) Swept-back plan form; $\lambda=0$; $\frac{c_r}{l}=0.5$.

(g) Notched triangular plan form.

FIGURE 9.—Concluded.

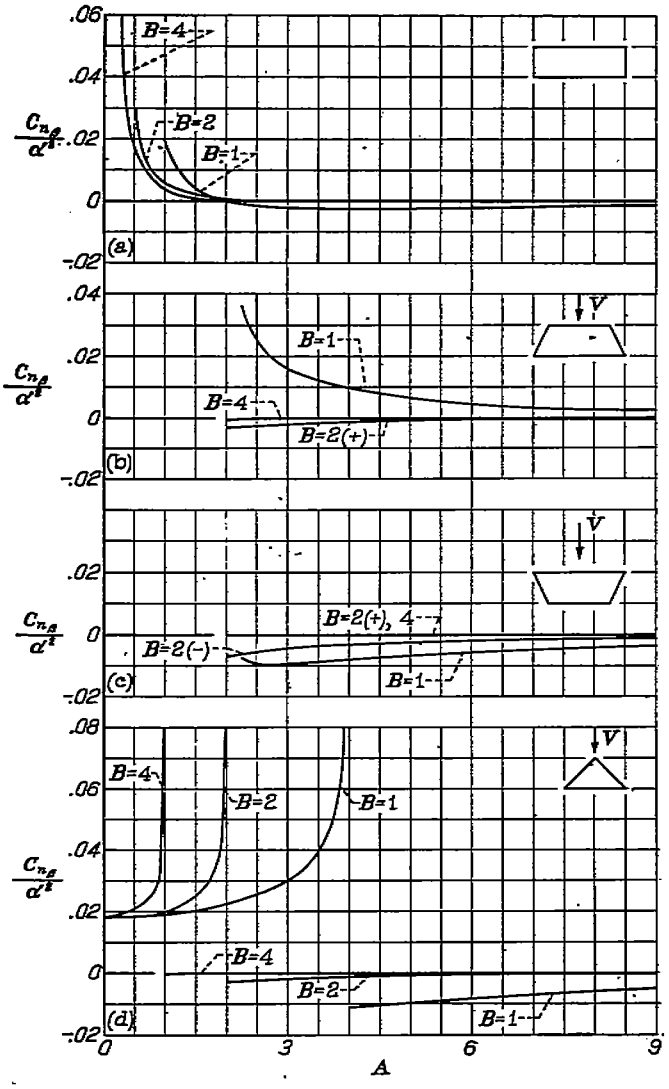

(a) Rectangular plan form.

(b) Trapezoidal plan form; $m=0.5$.

(c) Trapezoidal plan form; $m=-0.5$.

(d) Triangular plan form. Apex forward.

FIGURE 10.—Variation of yawing-moment-due-to-sideslip derivative with aspect ratio.

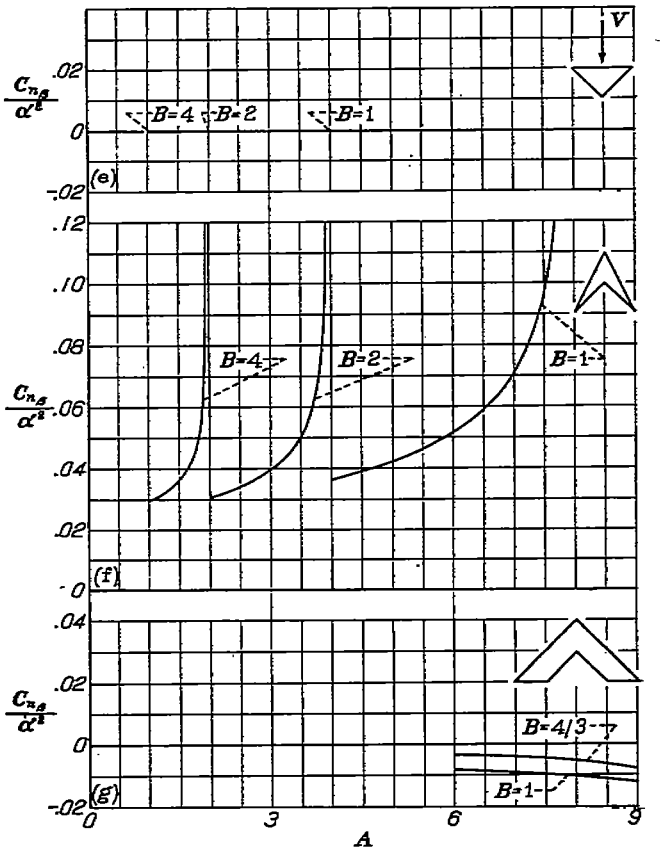

(e) Triangular plan form. Base forward. (See footnote, table II.)

(f) Swept-back plan form; $\lambda=0$; $\frac{c_r}{l}=0.5$.

(g) Notched triangular plan form; $m=3/2$.

FIGURE 10.—Concluded.

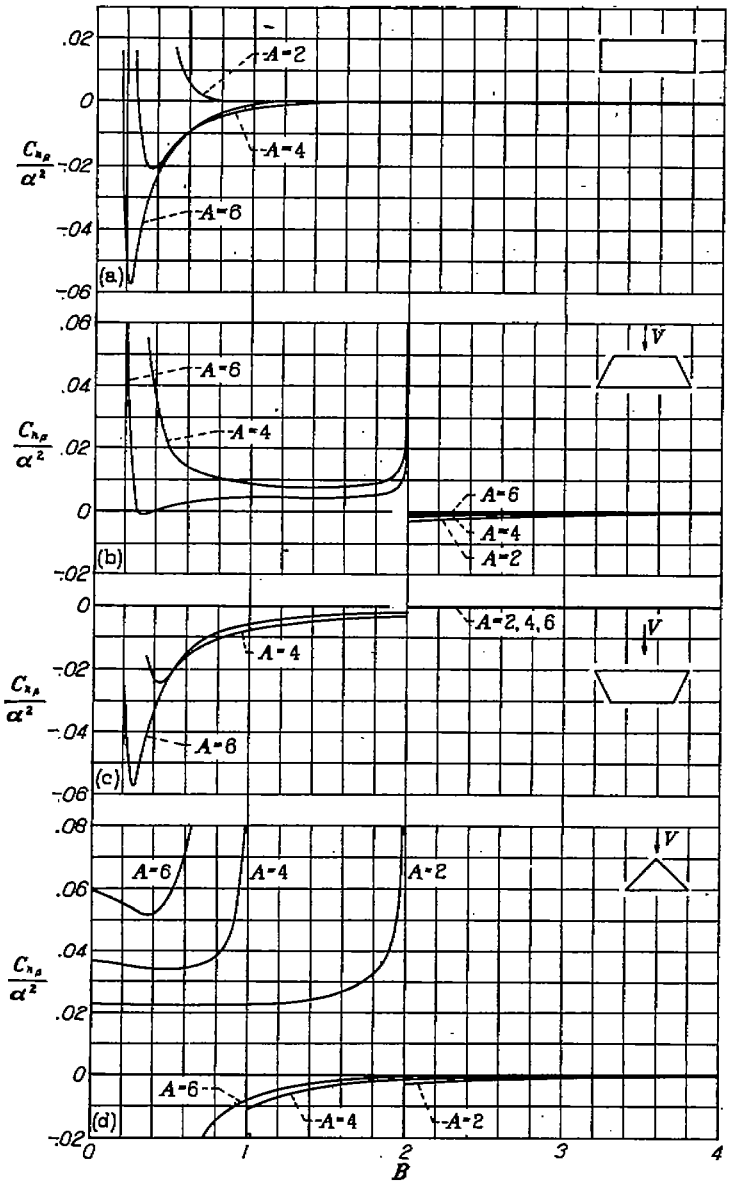

(a) Rectangular plan form.

(b) Trapezoidal plan form; $m=0.5$.

(c) Trapezoidal plan form; $m=-0.5$.

(d) Triangular plan form. Apex forward.

FIGURE 11.—Variation of yawing-moment-due-to-sideslip derivative with Mach number parameter B.

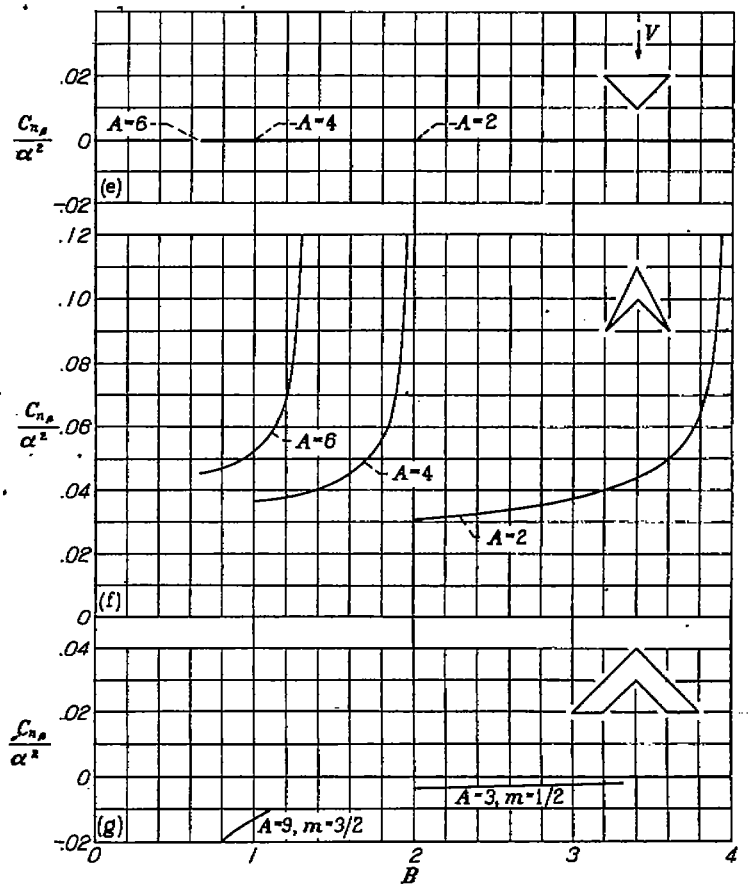

(e) Triangular plan form. Base forward. (See footnote, table II.)

(f) Swept-back plan form; $\lambda=0$; $\frac{c_r}{l}=0.5$.

(g) Notched triangular plan form.

FIGURE 11.—Concluded.

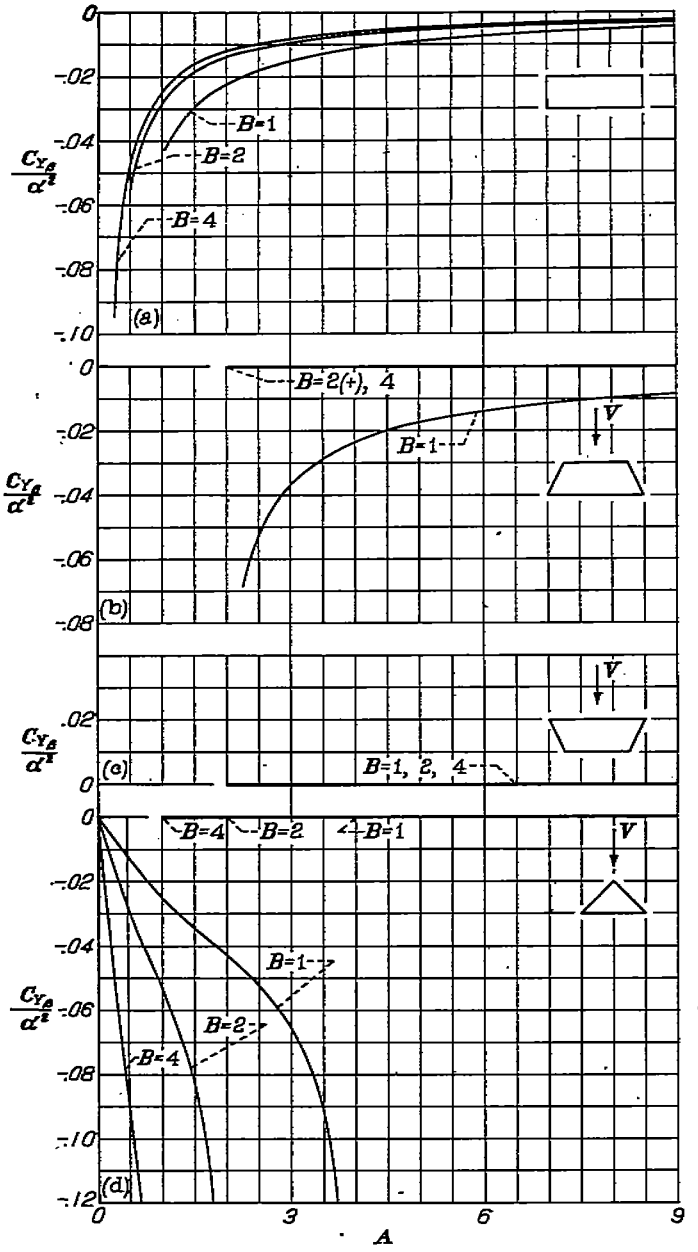

(a) Rectangular plan form.

(b) Trapezoidal plan form; $m=0.5$.

(c) Trapezoidal plan form; $m=-0.5$.

(d) Triangular plan form. Apex forward. (See footnote, table II.)

FIGURE 12.—Variation of side-force-due-to-sideslip derivative with aspect ratio.

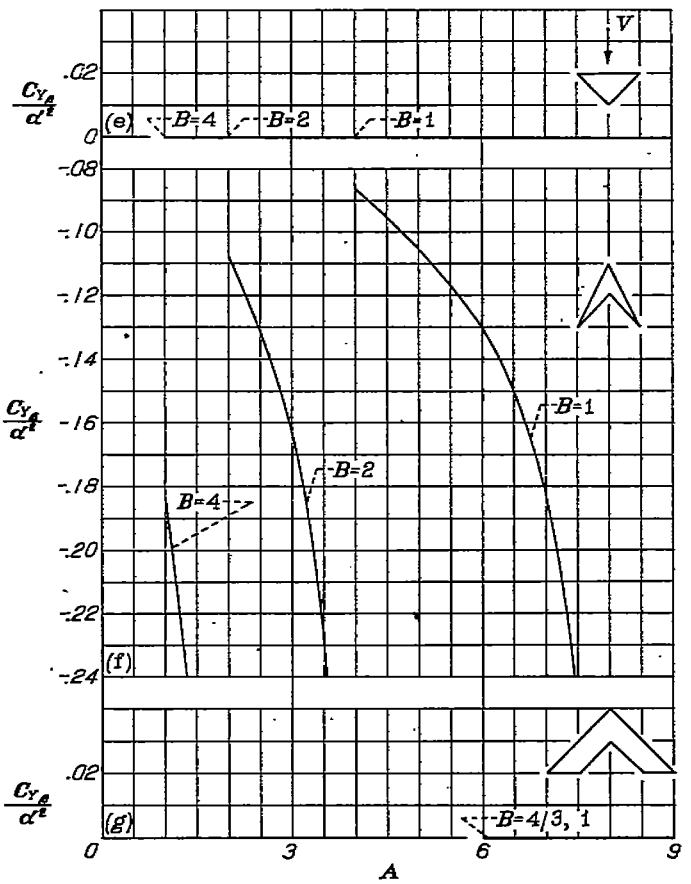

(e) Triangular plan form. Base forward. (See footnote, table II.)

(f) Swept-back plan form; $\lambda=0$; $\frac{c_r}{l}=0.5$.

(g) Notched triangular plan form; $m=3/2$.

FIGURE 12.—Concluded.

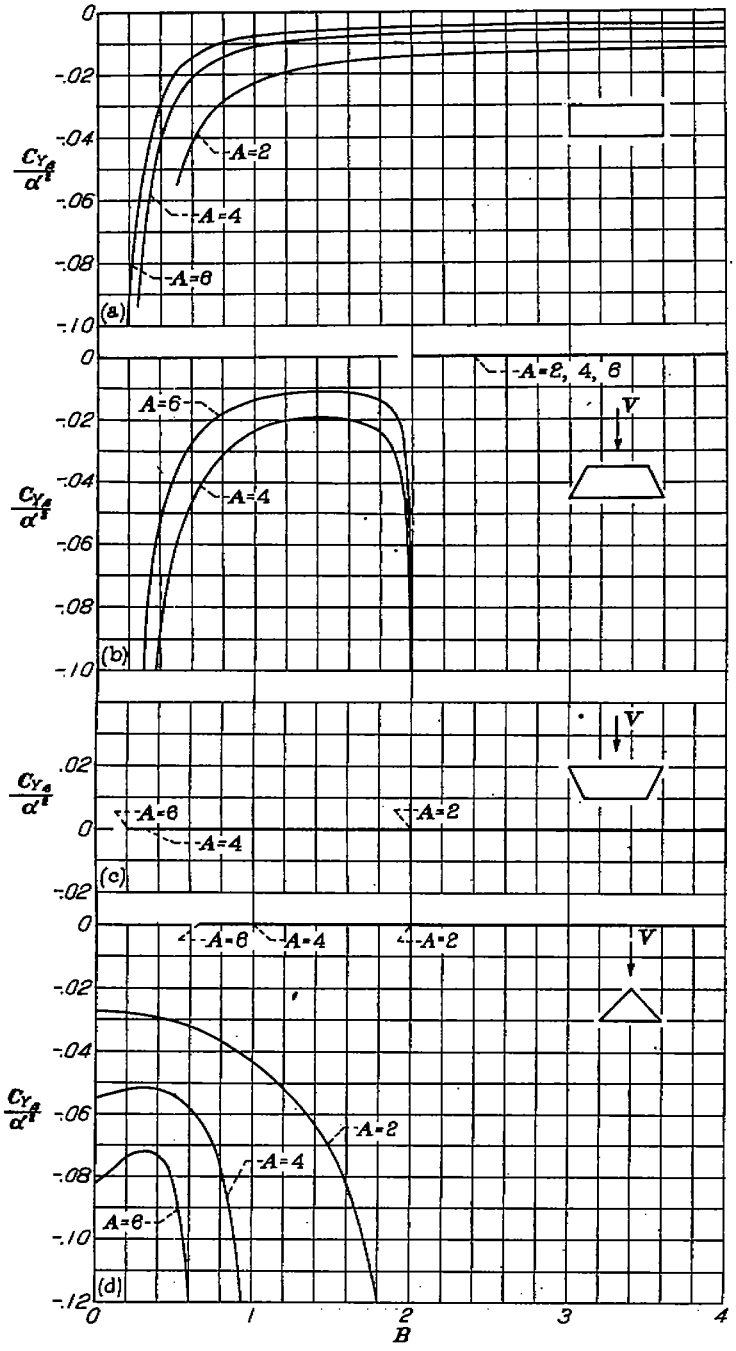

(a) Rectangular plan form.

(b) Trapezoidal plan form; $m=0.5$.

(c) Trapezoidal plan form; $m=-0.5$. (See footnote, table II.)

(d) Triangular plan form. Apex forward. (See footnote, table II.)

FIGURE 13.—Variation of side-force-due-to-sideslip derivative with Mach number parameter B.

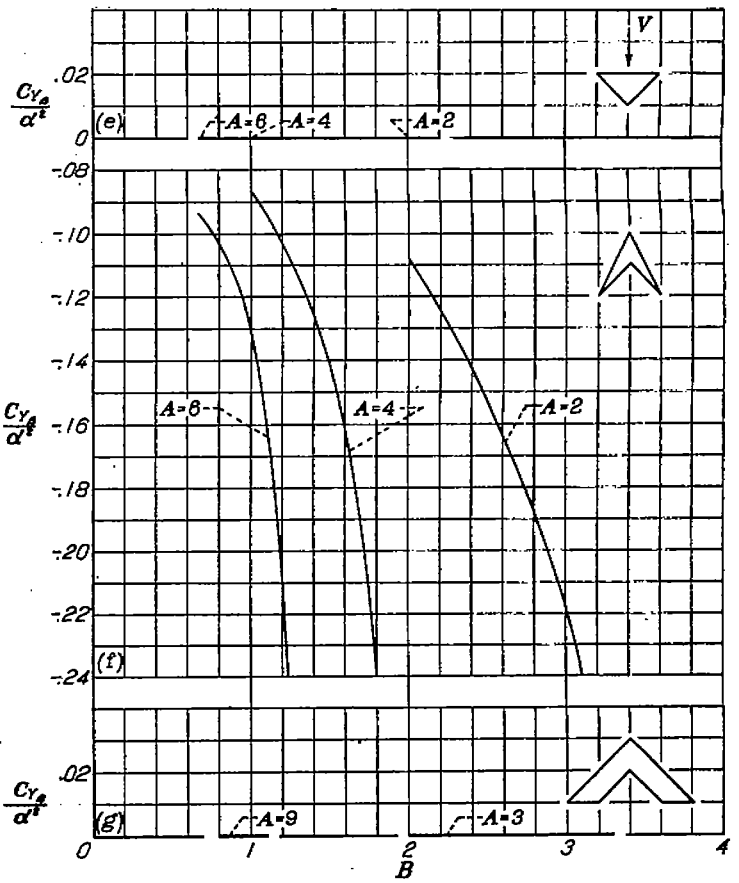

(e) Triangular plan form. Base forward. (See footnote, table II.)

(f) Swept-back plan form; $\lambda=0$; $\frac{c_r}{l}=0.5$.

(g) Notched triangular plan form.

FIGURE 13.—Concluded.

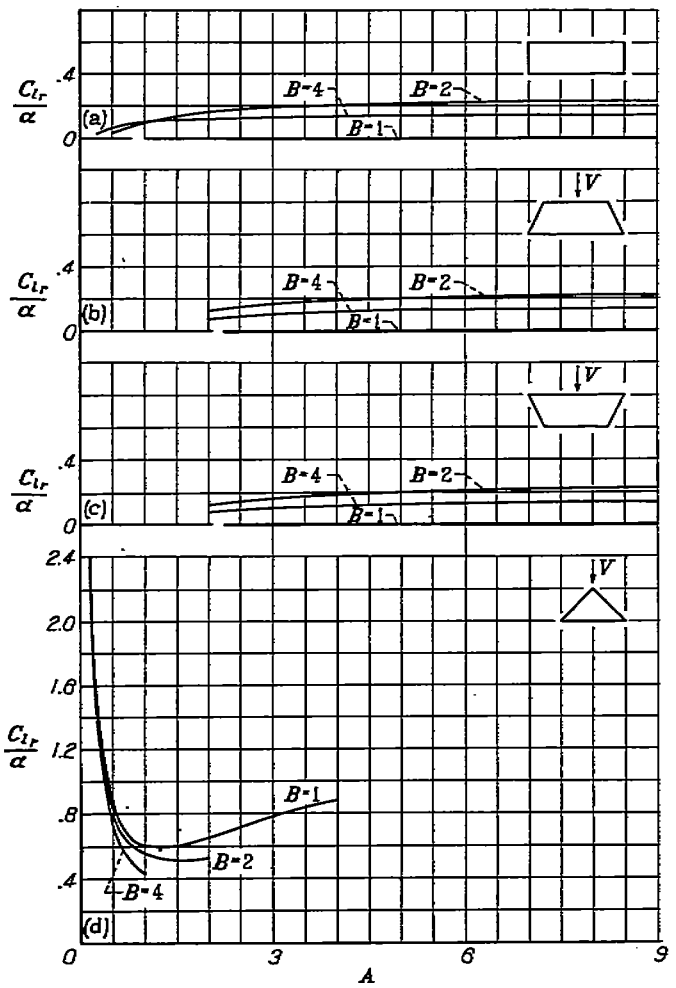

(a) Rectangular plan form.

(b) Trapezoidal plan form; $m=0.5$.

(c) Trapezoidal plan form; $m=-0.5$.

(d) Triangular plan form. Apex forward.

FIGURE 14.—Variation of rolling-moment-due-to-yawing derivative with aspect ratio.

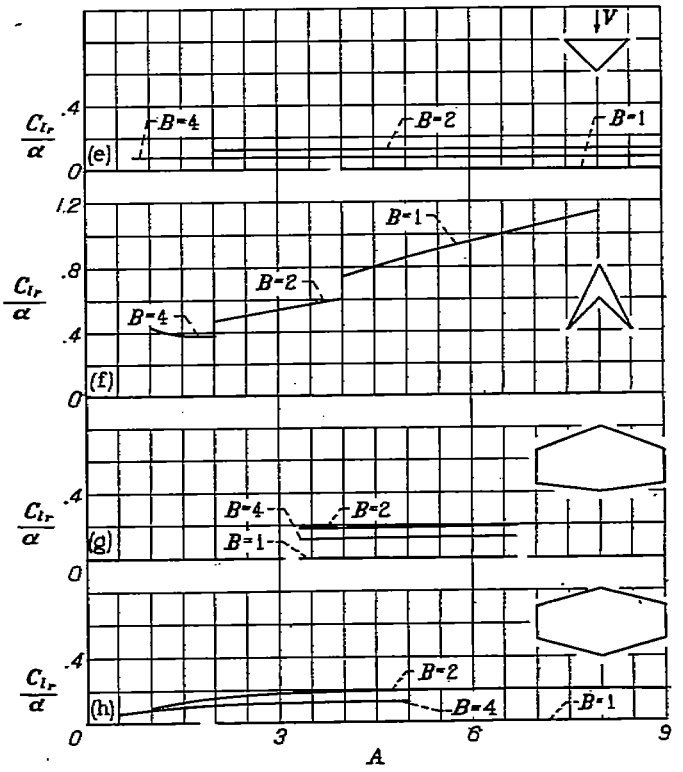

(e) Triangular plan form. Base forward.

(f) Swept-back plan form; $\lambda=0$; $\frac{c_r}{l}=0.5$.

(g) Unswept hexagonal plan form; $\lambda=0.5$; $m=5$.

(h) Unswept hexagonal plan form; $\lambda=0.5$; $Bm=3B\sqrt{2}$.

FIGURE 14.—Concluded.

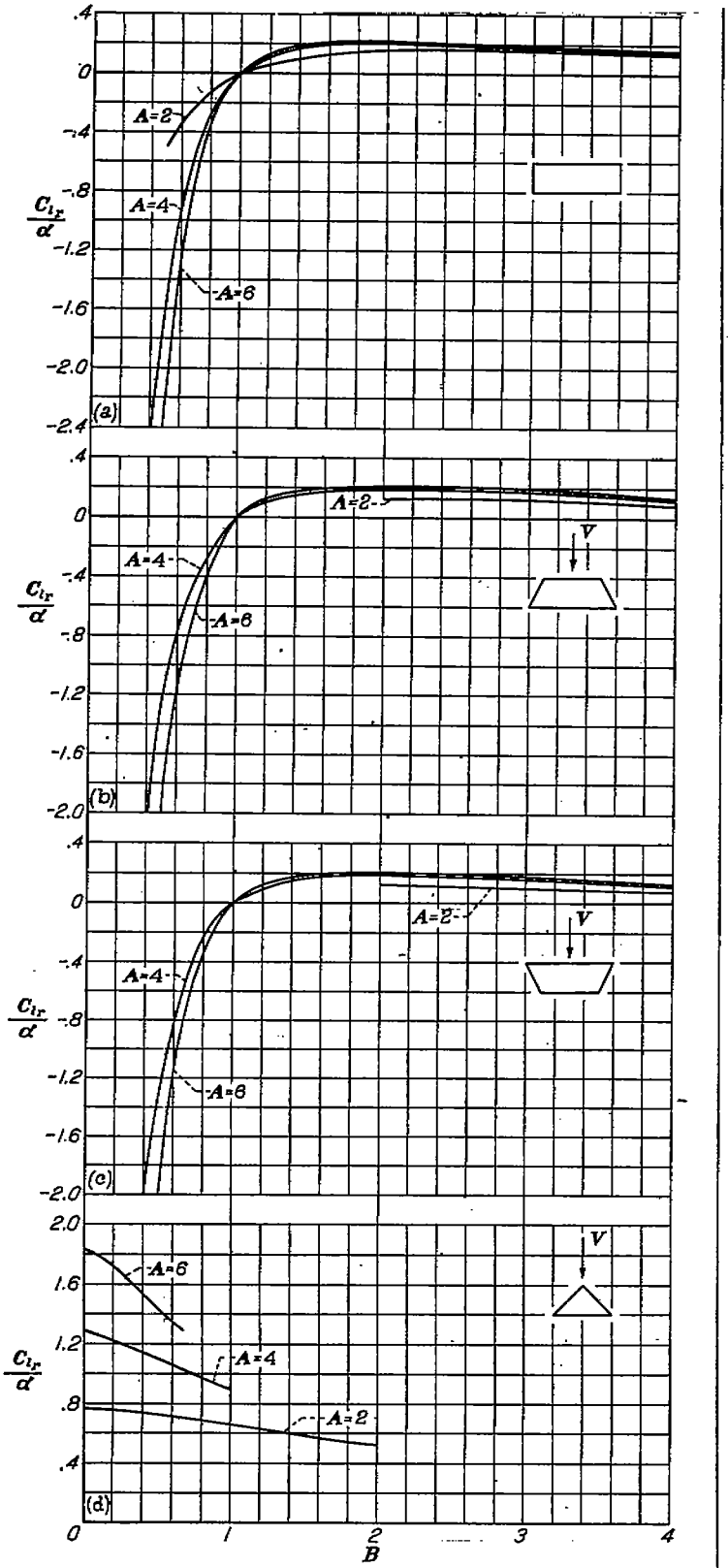

(a) Rectangular plan form.

(b) Trapezoidal plan form; $m=0.5$.

(c) Trapezoidal plan form; $m=-0.5$.

(d) Triangular plan form. Apex forward.

FIGURE 15.—Variation of rolling-moment-due-to-yawing derivative with Mach number parameter B.

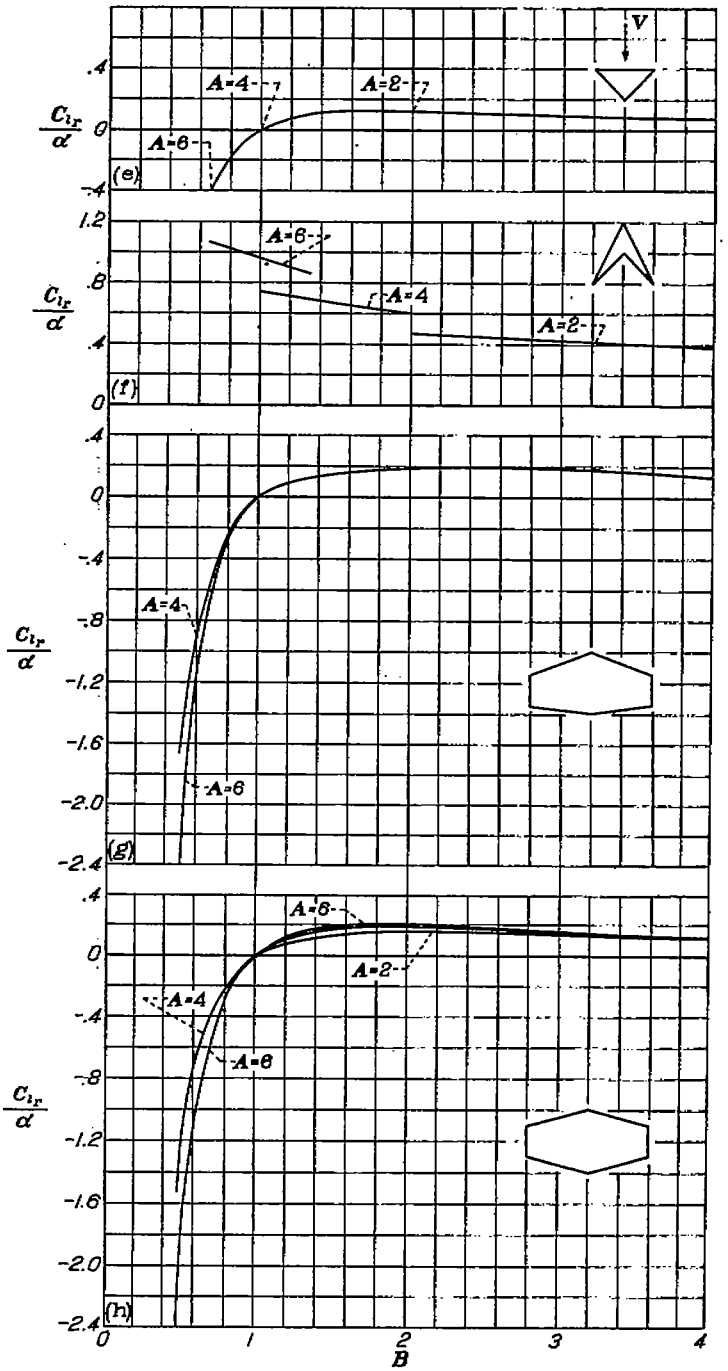

(e) Triangular plan form. Base forward. (See footnote, table II.)

(f) Swept-back plan form; $\lambda=0$; $\frac{c_r}{l}=0.5$.

(g) Unswept hexagonal plan form; $\lambda=0.5$; $m=5$.

(h) Unswept hexagonal plan form; $\lambda=0.5$; $Bm=3BA/2$.

FIGURE 15.—Concluded.

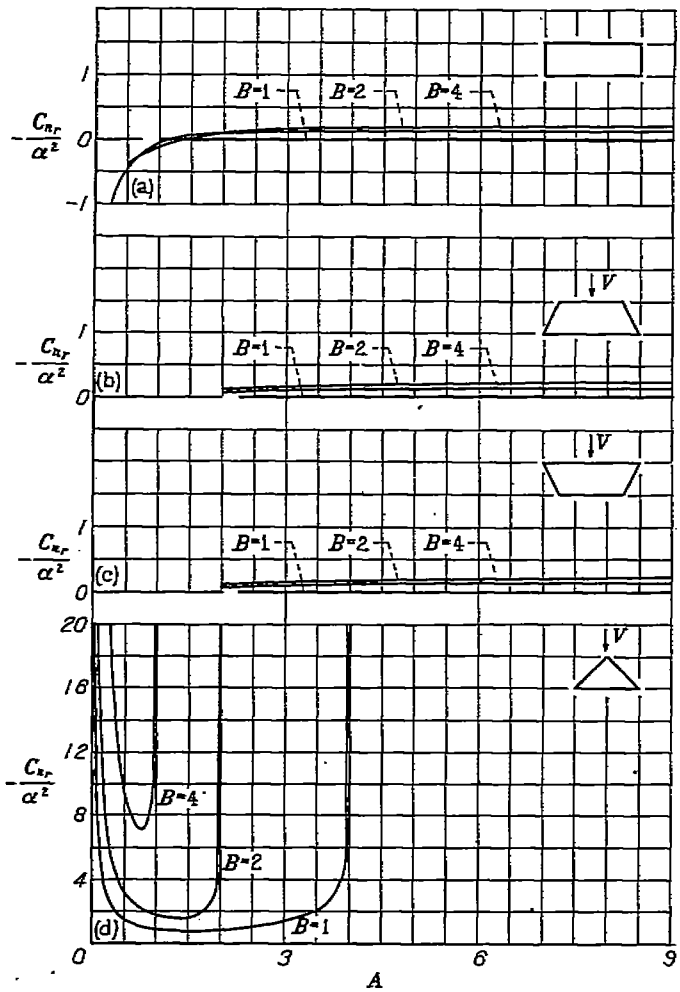

(a) Rectangular plan form.

(b) Trapezoidal plan form; $m=0.5$.

(c) Trapezoidal plan form; $m=-0.5$.

(d) Triangular plan form. Apex forward.

FIGURE 16.—Variation of damping-in-yaw derivative with aspect ratio.

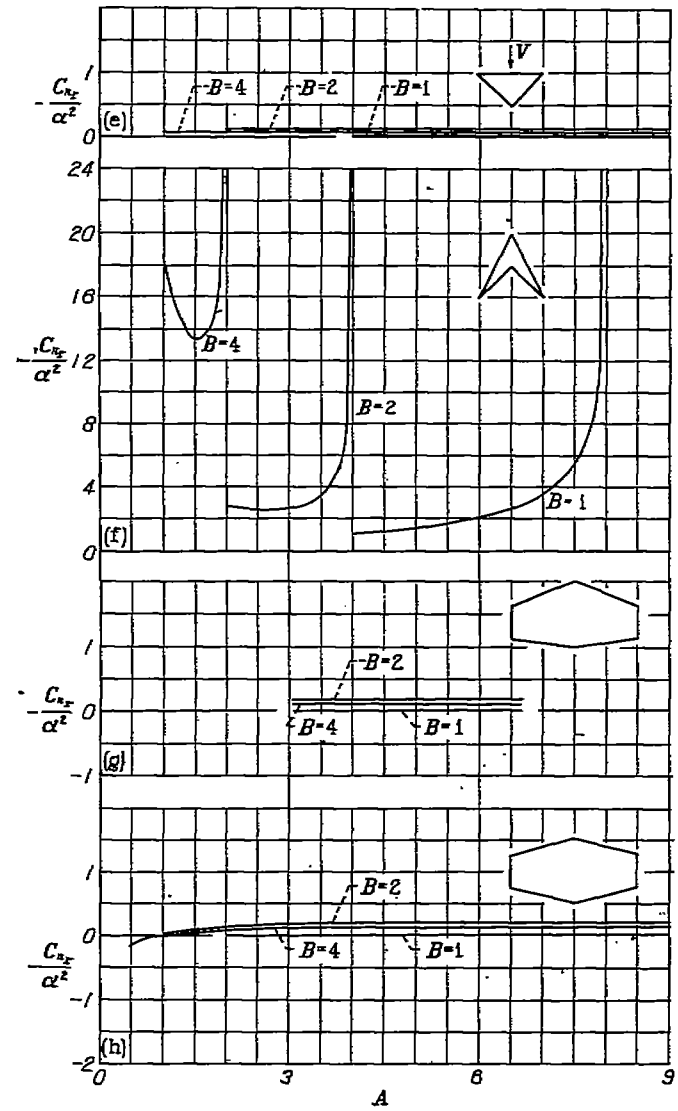

(e) Triangular plan form. Base forward.

(f) Swept-back plan form; $\lambda=0$; $\frac{c_r}{l}=0.5$.

(g) Unswept hexagonal plan form; $\lambda=0.5$; $m=5$.

(h) Unswept hexagonal plan form; $\lambda=0.5$; $Bm=3B.4/2$.

FIGURE 16.—Concluded.

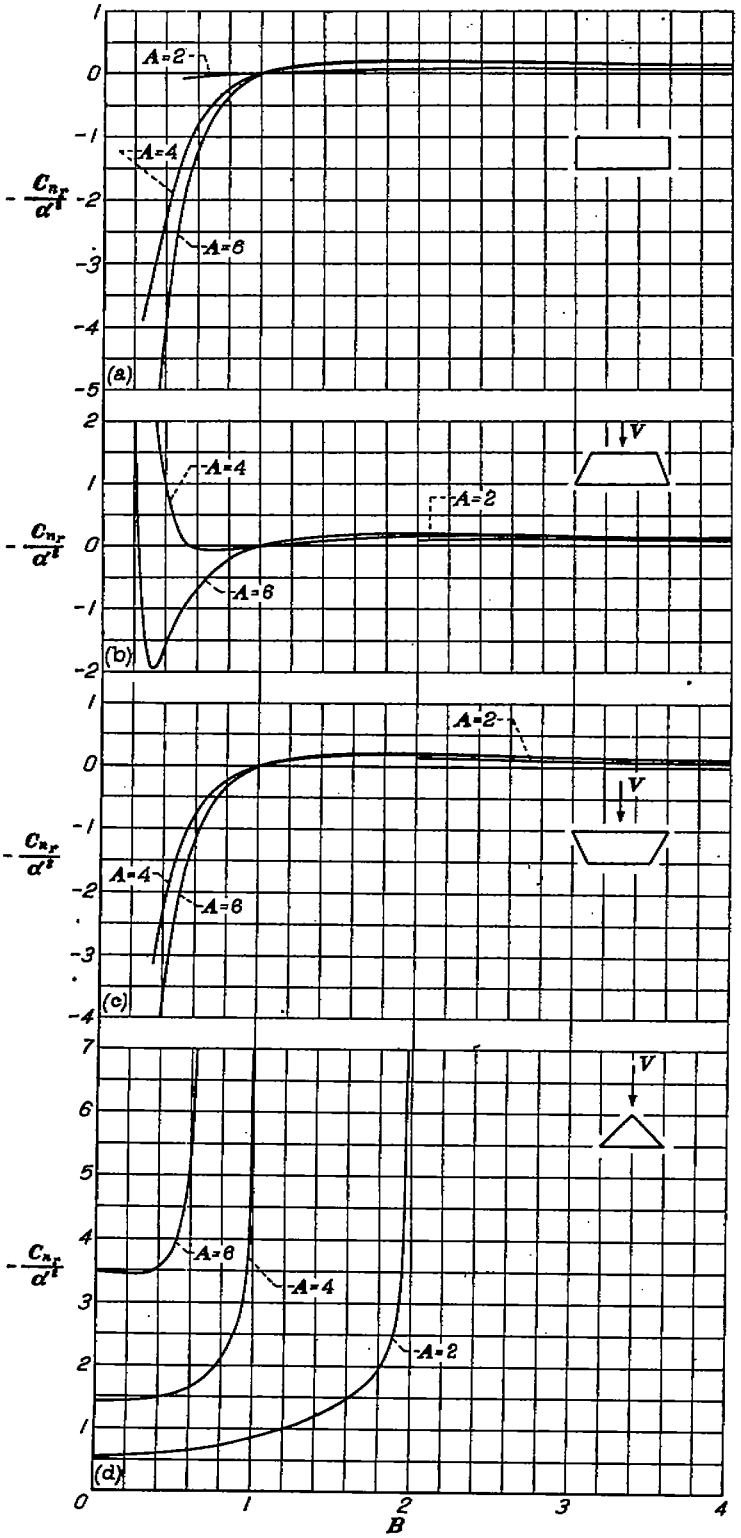

(a) Rectangular plan form.

(b) Trapezoidal plan form; $m=0.5$.

(c) Trapezoidal plan form; $m=-0.5$.

(d) Triangular plan form. Apex forward.

Figure 17.—Variation of damping-in-yaw derivative with Mach number parameter B.

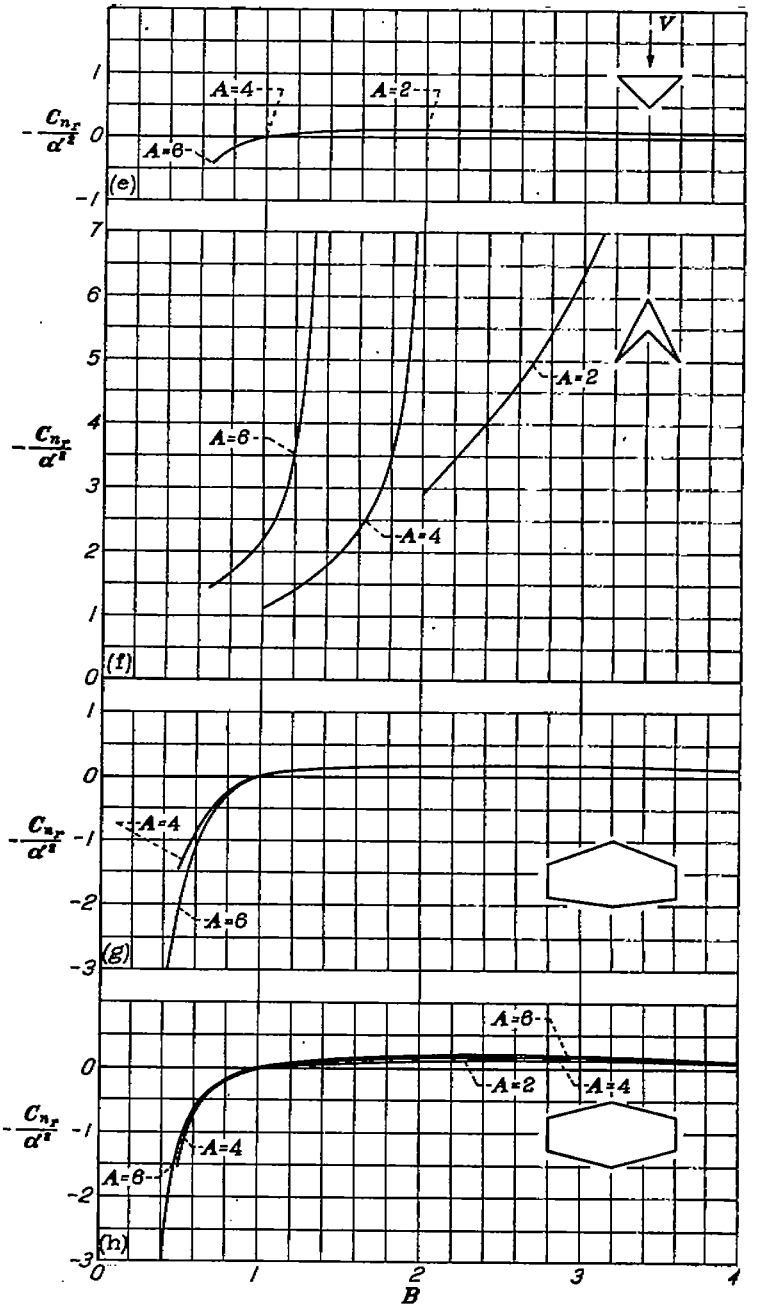

(e) Triangular plan form. Base forward. (See footnote, table II.)

(f) Swept-back plan form; $\lambda=0$; $\frac{c_r}{l}=0.5$.

(g) Unswept hexagonal plan form; $\lambda=0.5$; $m=5$.

(h) Unswept hexagonal plan form; $\lambda=0.5$; $Bm=3BA/\pi$.

FIGURE 17.—Concluded.

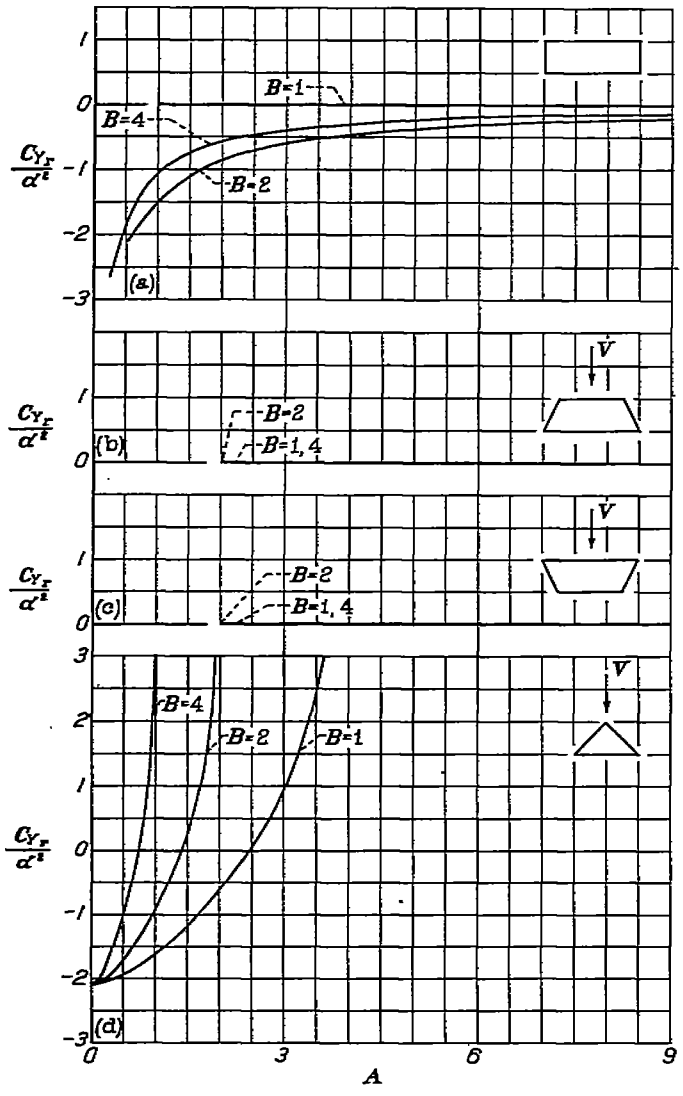

(a) Rectangular plan form.

(b) Trapezoidal plan form; $m=0.5$. (See footnote, table II.)

(c) Trapezoidal plan form; $m=-0.5$. (See footnote, table II.)

(d) Triangular plan form. Apex forward.

FIGURE 18.—Variation of side-force-due-to-yawing derivative with aspect ratio.

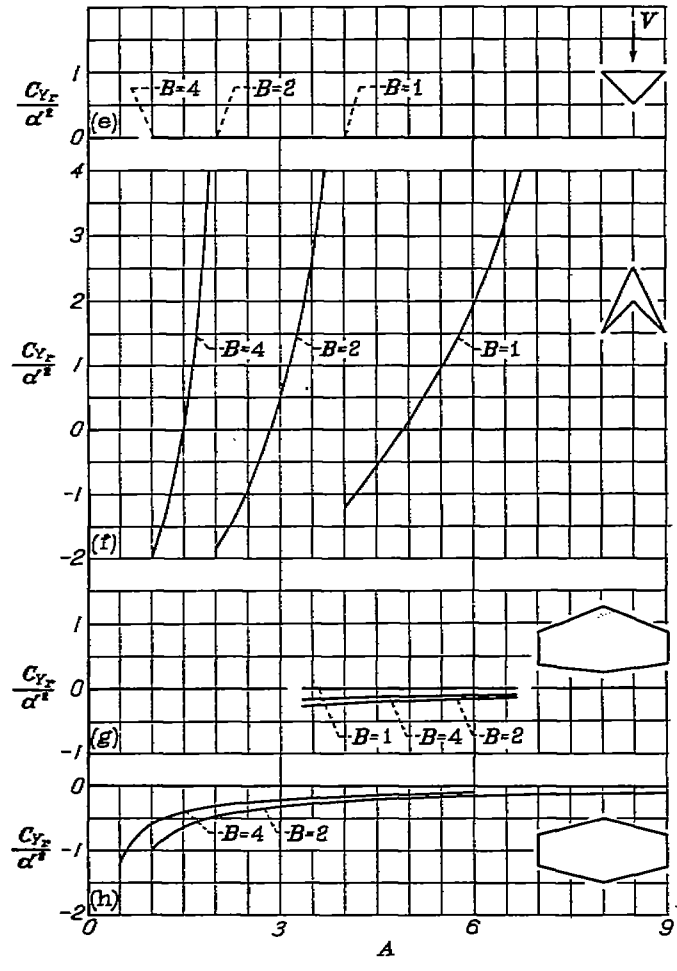

(e) Triangular plan form. Base forward. (See footnote, table II.)

(f) Swept-back plan form; $\lambda=0$; $\frac{c_r}{l}=0.5$.

(g) Unswept hexagonal plan form; $\lambda=0.5$; $m=5$.

(h) Unswept hexagonal plan form; $\lambda=0.5$; $Bm=3B.4/2$.

FIGURE 18.—Concluded.

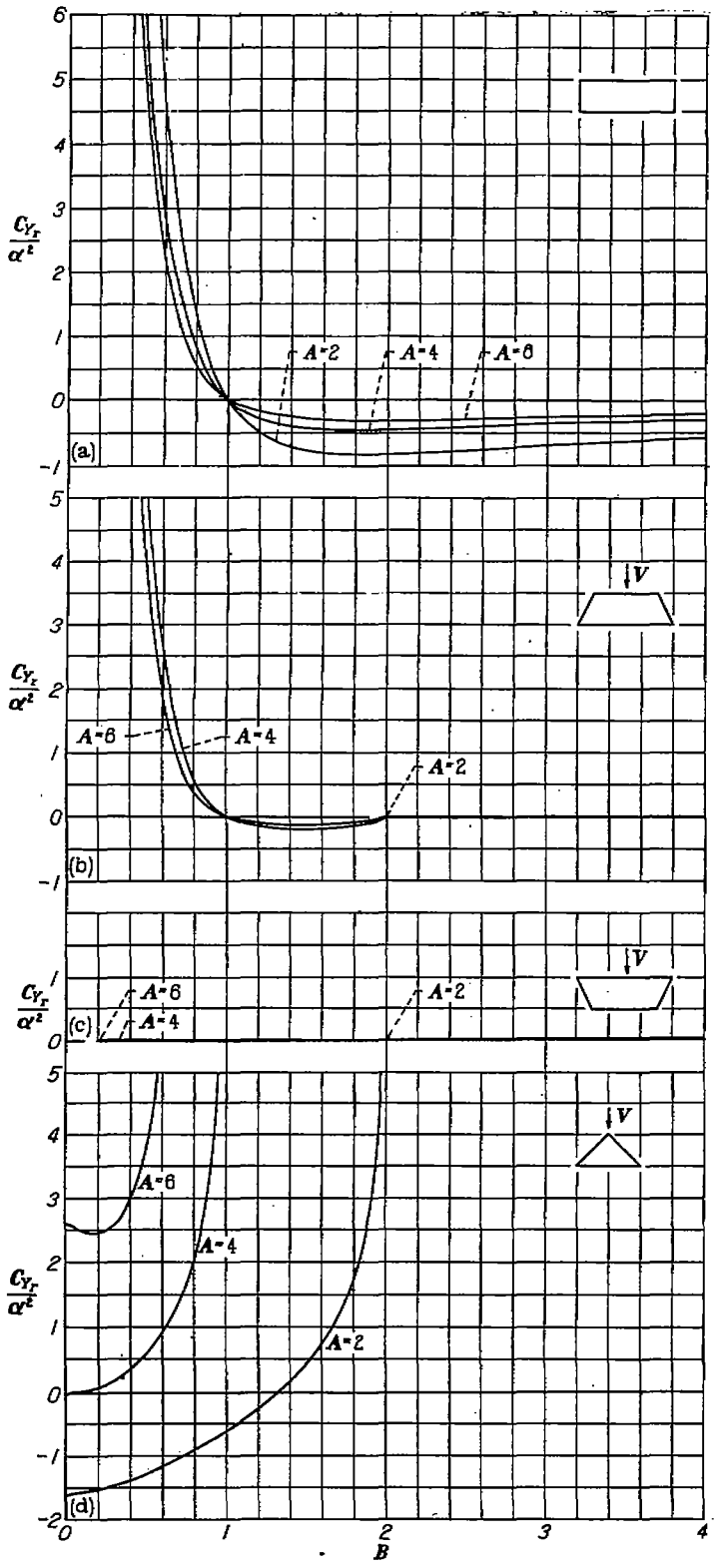

(a) Rectangular plan form.

(b) Trapezoidal plan form; $m=0.5$.

(c) Trapezoidal plan form; $m=-0.5$. (See footnote, table II.)

(d) Triangular plan form. Apex forward.

FIGURE 19.—Variation of side-force-due-to-yawing derivative with Mach number parameter B.

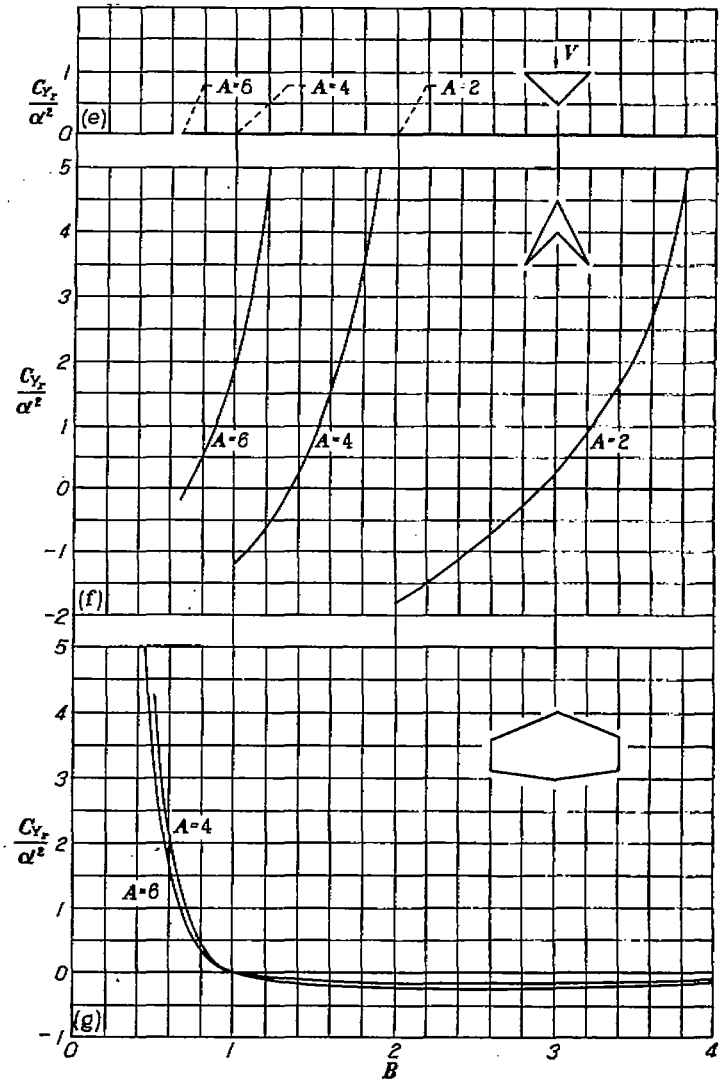

(e) Triangular plan form. Base forward. (See footnote, table II.)

(f) Swept-back plan form; $\lambda=0$; $\frac{c_r}{l}=0.5$.

(g) Unswept hexagonal plan form; $\lambda=0.5$; $m=5$.

FIGURE 19.—Continued.

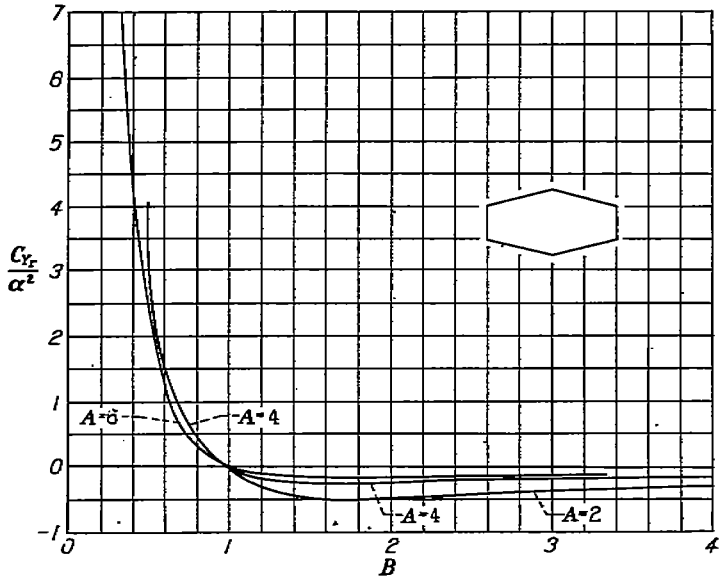

FIGURE 19.—Concluded. (h) Unswept hexagonal plan form; $\lambda=0.5$; $Bm=3BA/2$.

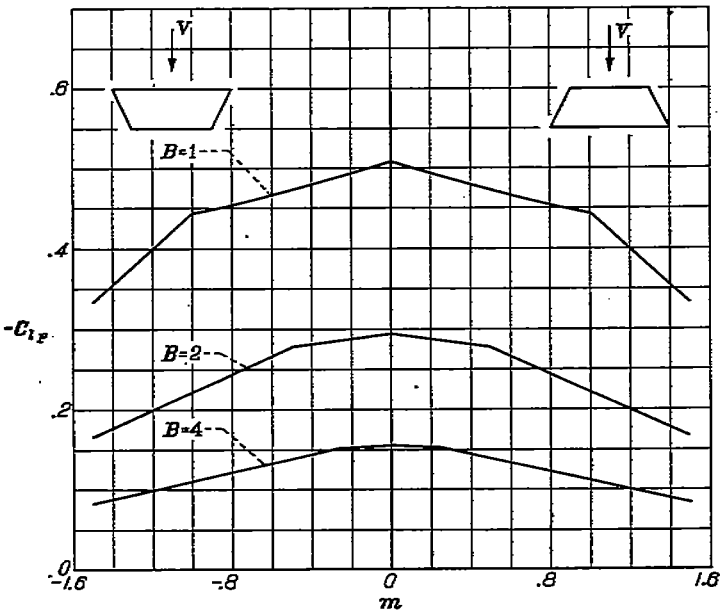

FIGURE 20.—Variation of damping-in-roll derivative with tip slope for trapezoidal plan forms; $A=6$.

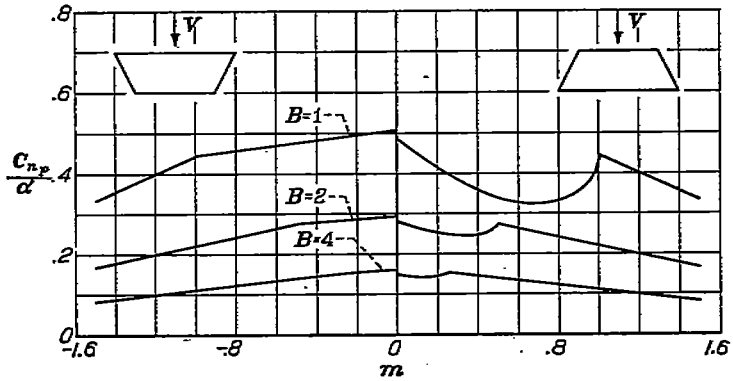

FIGURE 21.—Variation of yawing-moment-due-to-roll derivative with tip slope for trapezoidal plan forms; $A=6$.

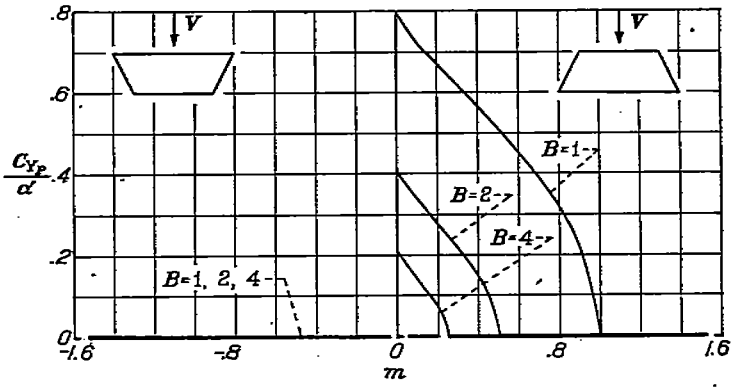

FIGURE 22.—Variation of side-force-due-to-rolling derivative with tip slope for trapezoidal plan forms; $A=6$.

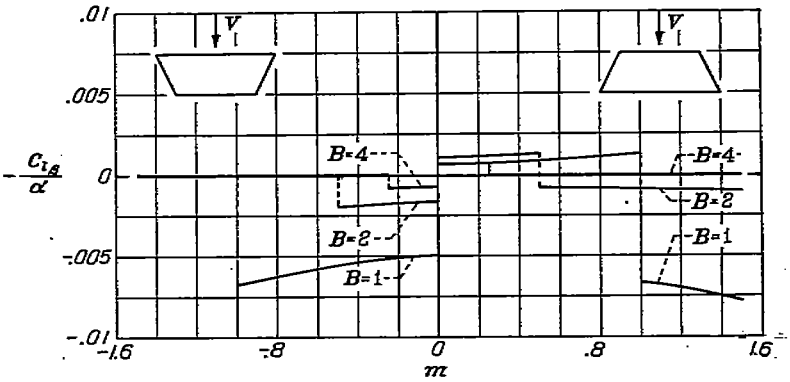

FIGURE 23.—Variation of rolling-moment-due-to-sideslip derivative with tip slope for trapezoidal plan forms; $A=6$.

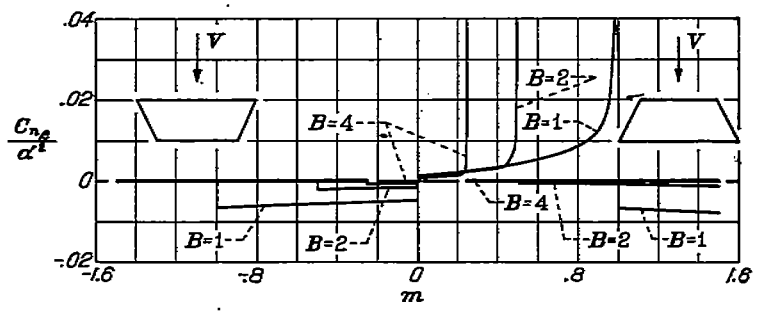

FIGURE 24.—Variation of yawing-moment-due-to-sideslip derivative with tip slope for trapezoidal plan forms; $A=6$.

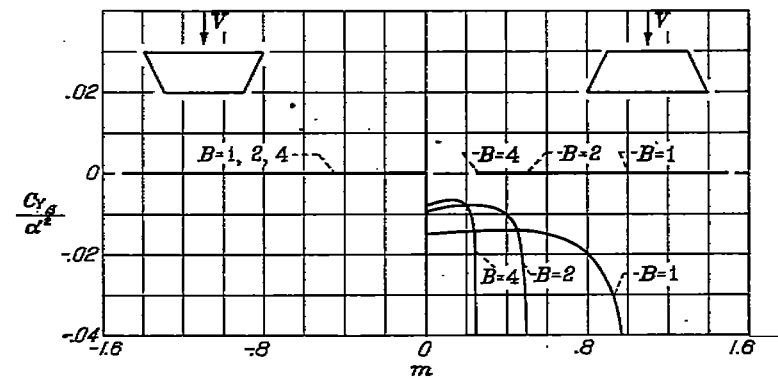

FIGURE 25.—Variation of side-force-due-to-sideslip derivative with tip slope for trapezoidal plan forms; $A=6$. (See footnote, table II.)

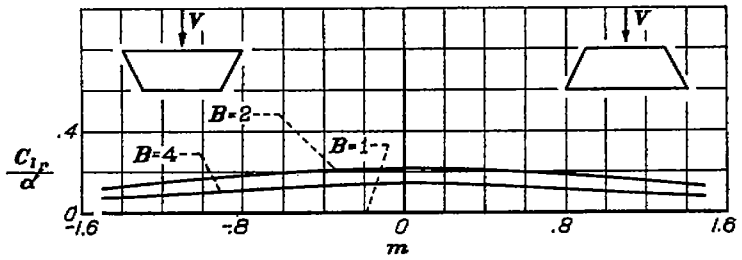

FIGURE 26.—Variation of rolling-moment-due-to-yawing derivative with tip slope for trapezoidal plan forms; $A=6$.

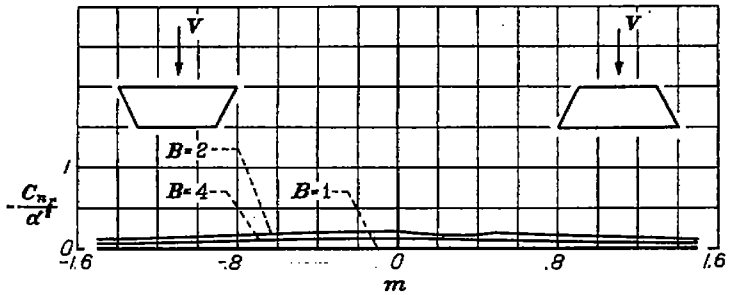

FIGURE 27.—Variation of damping-in-yaw derivative with tip slope for trapezoidal plan forms; $A=6$.

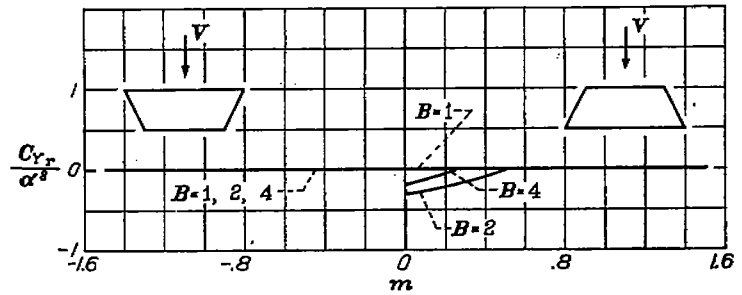

FIGURE 28.—Variation of side-force-due-to-yawing derivative with tip slope for trapezoidal plan forms; $A=6$.

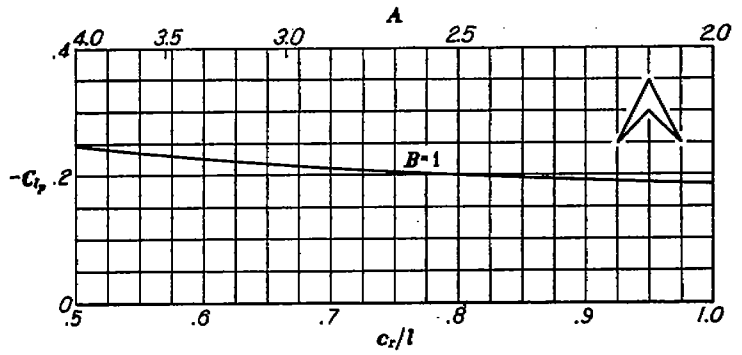

FIGURE 29.—Variation of damping-in-roll derivative with ratio of root chord to over-all length of swept-back plan form; $m=0.5$.

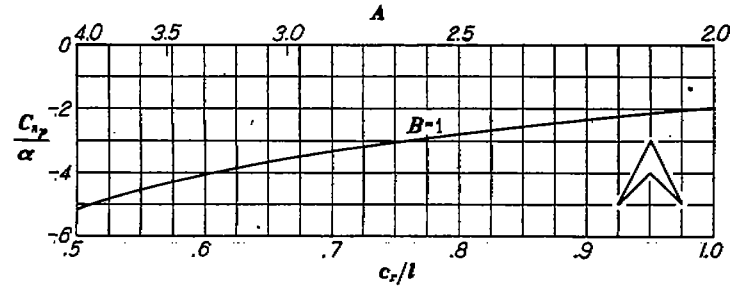

FIGURE 30.—Variation of yawing-moment-due-to-roll derivative with ratio of root chord to over-all length of swept-back plan form; $m=0.5$.

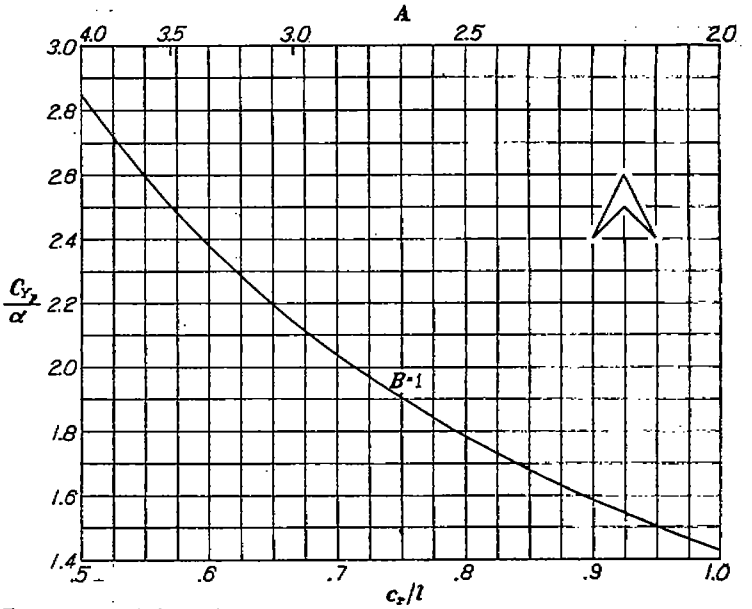

FIGURE 31.—Variation of side-force-due-to-roll derivative with ratio of root chord to over-all length of swept-back plan form; $m=0.5$.

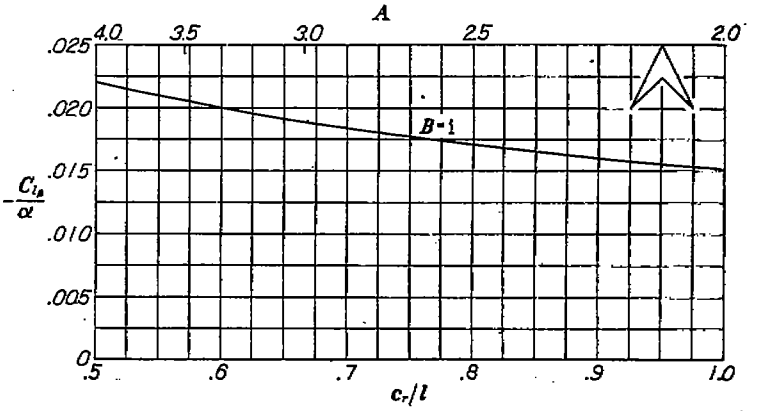

FIGURE 32.—Variation of rolling-moment-due-to-sideslip derivative with ratio of root chord to over-all length of swept-back plan form; $m=0.5$.

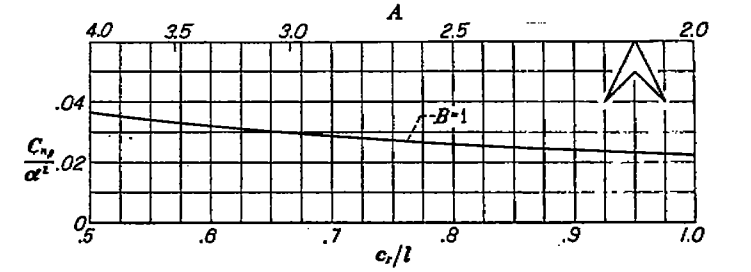

FIGURE 33.—Variation of yawing-moment-due-to-sideslip derivative with ratio of root chord to over-all length of swept-back plan form; $m=0.5$.

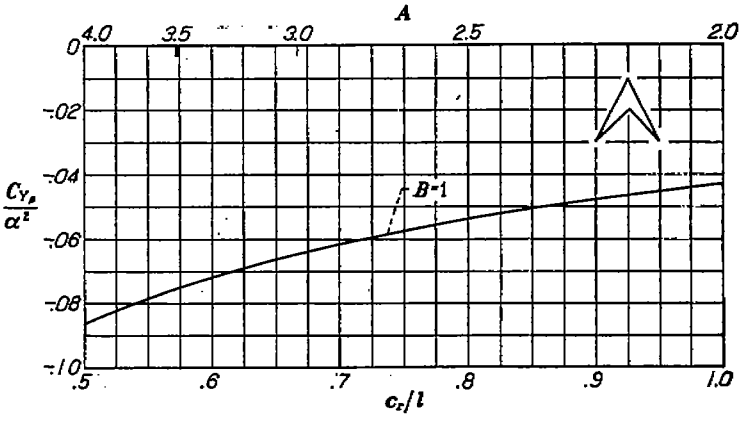

FIGURE 34.—Variation of side-force-due-to-sideslip derivative with ratio of root chord to over-all length of swept-back plan form; $m=0.5$.

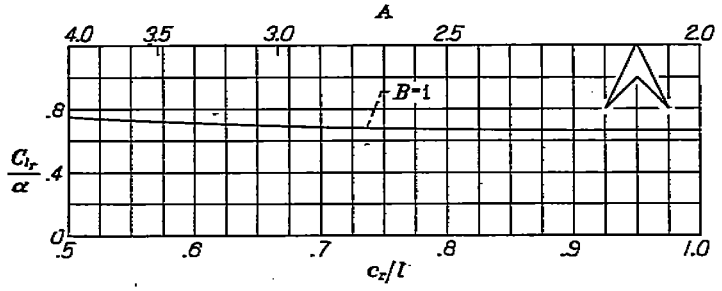

FIGURE 35.—Variation of rolling-moment-due-to-yawing derivative with ratio of root chord to over-all length of swept-back plan form; $m=0.5$.

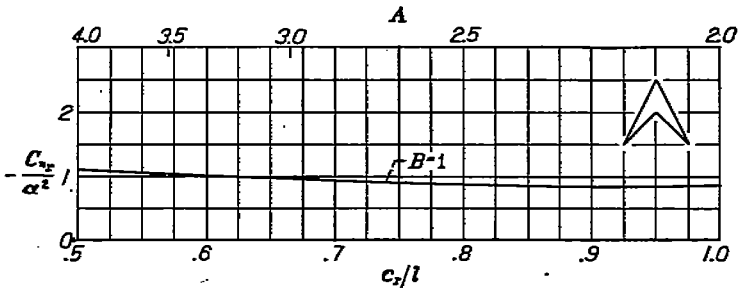

FIGURE 36.—Variation of damping-in-yaw derivative with ratio of root chord to over-all length of swept-back plan form; $m=0.5$.

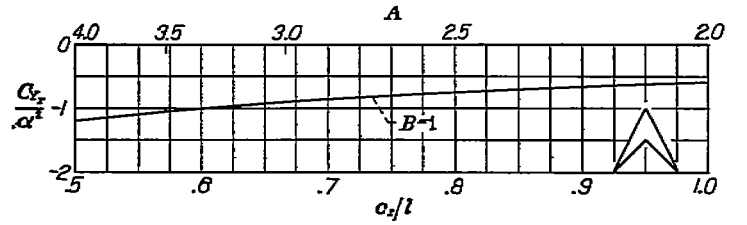

FIGURE 37.—Variation of side-force-due-to-yawing derivative with ratio of root chord to over-all length of swept-back plan form; $m=0.5$.

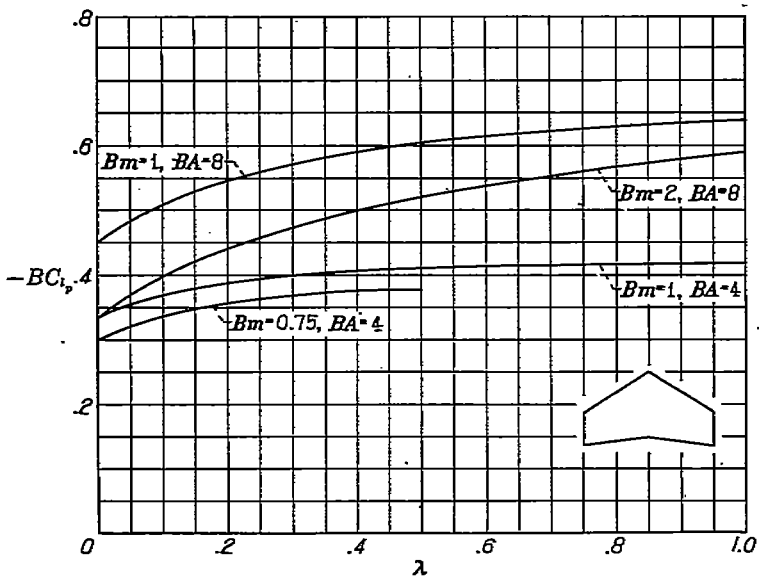

FIGURE 38.—Variation of damping-in-roll parameter with taper ratio for swept-back hexagonal plan form.

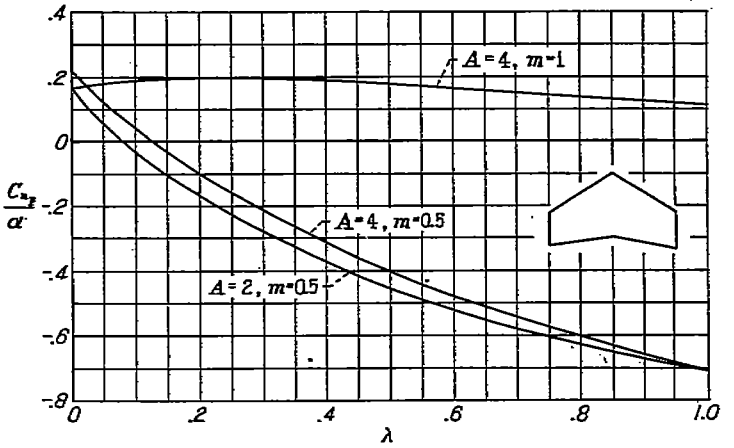

FIGURE 39.—Variation of yawing-moment-due-to-roll derivative with taper ratio for swept-back hexagonal plan form; $B=2$.

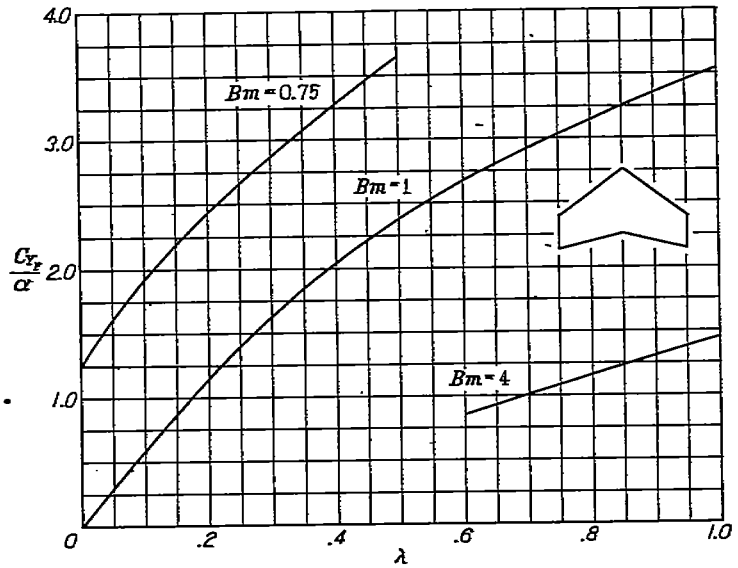

FIGURE 40.—Variation of side-force-due-to-roll derivative with taper ratio for swept-back plan form; $BA=4$.

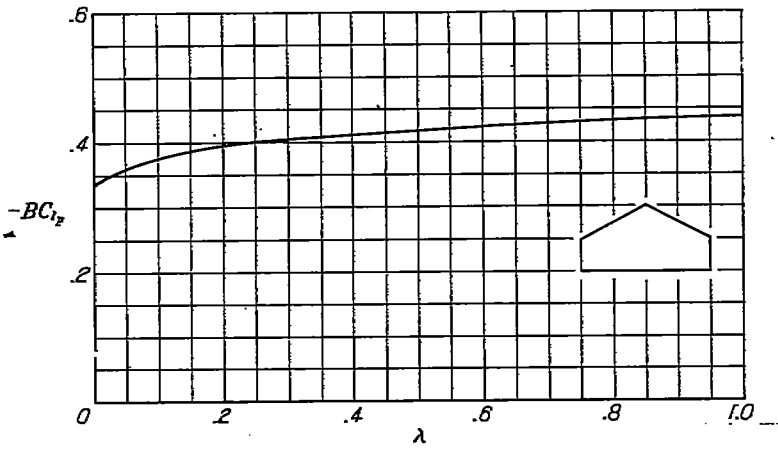

FIGURE 41.—Variation of damping-in-roll parameter with taper ratio for swept-back hexagonal plan form; $Bm=BA(1+\lambda)/4(1-\lambda)$; $BA=4$.

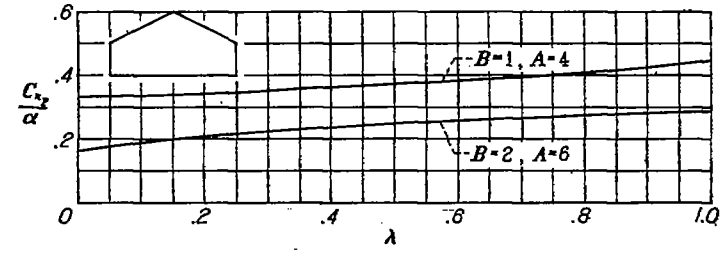

FIGURE 42.—Variation of yawing-moment-due-to-roll derivative with taper ratio for swept-back hexagonal plan form; $Bm=BA(1+\lambda)/4(1-\lambda)$.

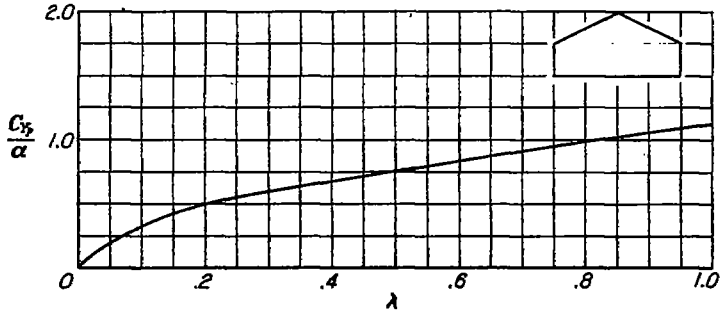

FIGURE 43.—Variation of side-force-due-to-roll derivative with taper ratio for swept-back hexagonal plan form. $Bm=BA(1+\lambda)/4(1-\lambda)$; $BA=4$.

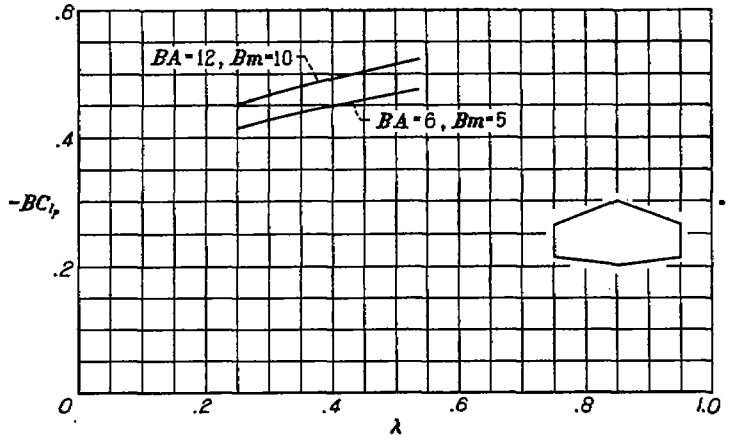

FIGURE 44.—Variation of damping-in-roll parameter with taper ratio for unswept hexagonal plan form.

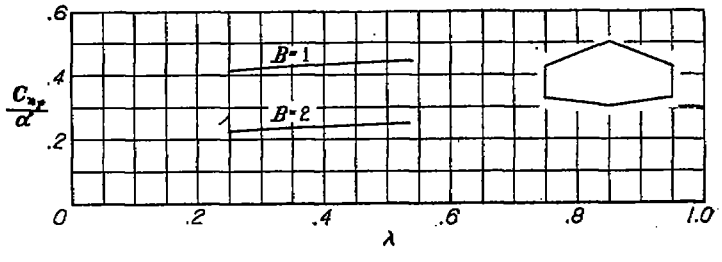

FIGURE 45.—Variation of yawing-moment-due-to-roll derivative with taper ratio for unswept hexagonal plan form; $A=6$; $m=5$.

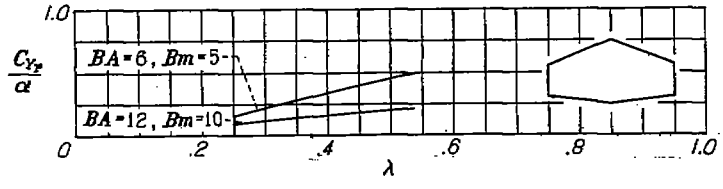

FIGURE 46.—Variation of side-force-due-to-roll derivative with taper ratio for unswept hexagonal plan form.

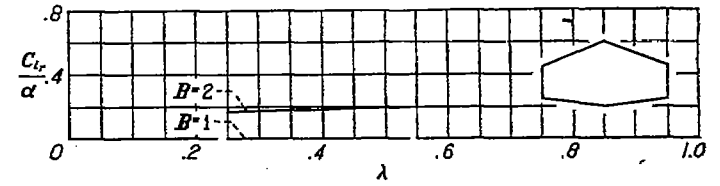

FIGURE 47.—Variation of rolling-moment-due-to-yawing derivative with taper ratio for unswept hexagonal plan form; $A=6$; $m=5$.

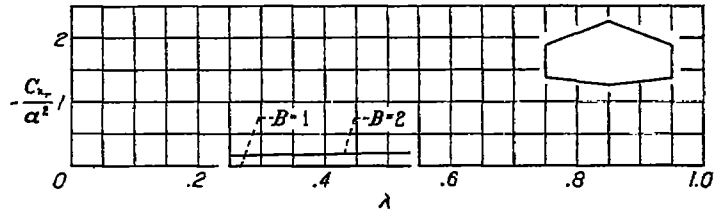

FIGURE 48.—Variation of damping-in-yaw derivative with taper ratio for unswept hexagonal plan form; $A=6$; $m=5$.

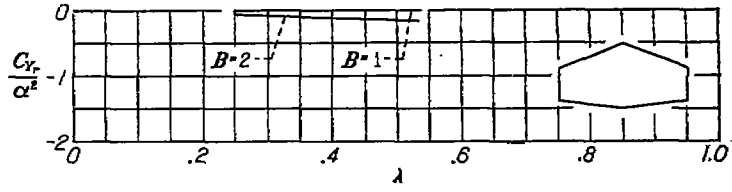

FIGURE 49.—Variation of side-force-due-to-yawing derivative with taper ratio for unswept hexagonal plan form; $A=6$; $m=5$.

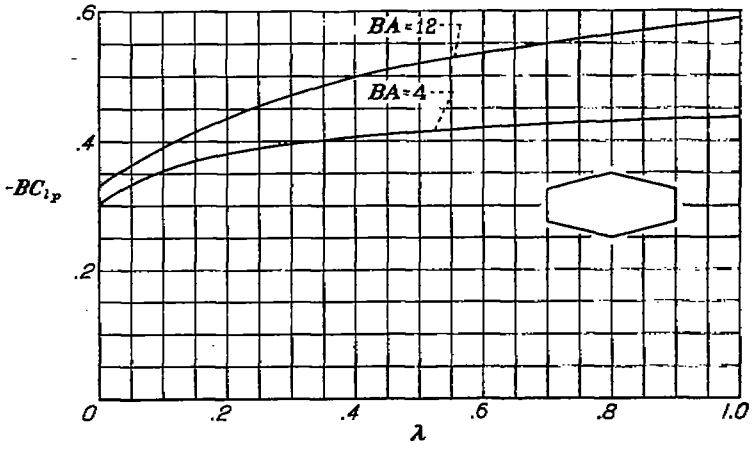

FIGURE 50.—Variation of damping-in-roll parameter with taper ratio for unswept hexagonal plan form; $Bm=BA(1+\lambda)/2(1-\lambda)$.

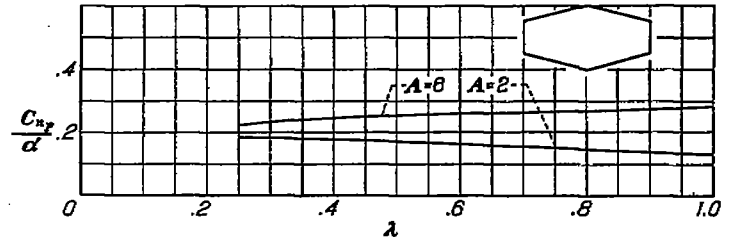

FIGURE 51.—Variation of yawing-moment-due-to-roll derivative with taper ratio for unswept hexagonal plan form; $B=2$; $Bm=BA(1+\lambda)/2(1-\lambda)$.

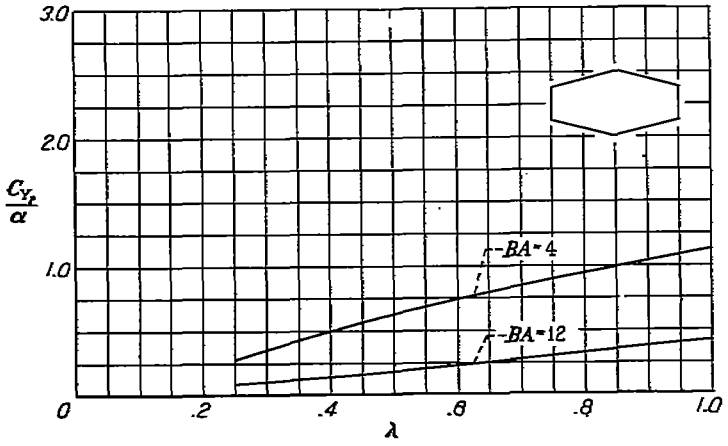

FIGURE 52.—Variation of side-force-due-to-roll derivative with taper ratio for unswept hexagonal plan form; $Bm=BA(1+\lambda)/2(1-\lambda)$.

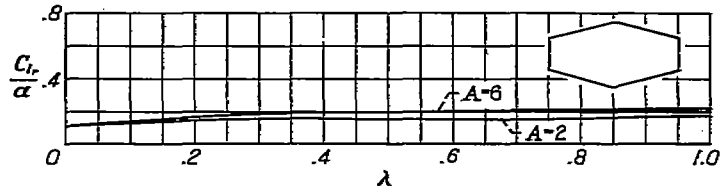

FIGURE 53.—Variation of rolling-moment-due-to-yawing derivative with taper ratio for unswept hexagonal plan form; $B=2$; $Bm=BA(1+\lambda)/2(1-\lambda)$..

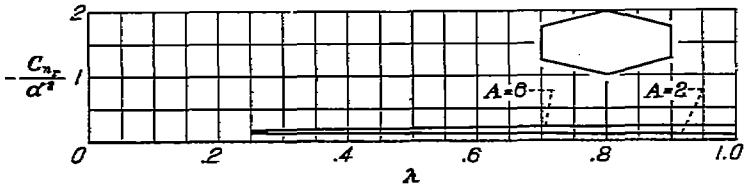

FIGURE 54.—Variation of damping-in-yaw derivative with taper ratio for unswept hexagonal plan form; $B=2$; $Bm=BA(1+\lambda)/2(1-\lambda)$.

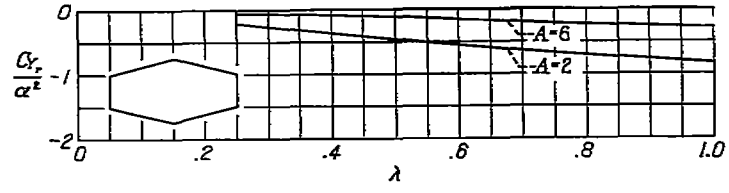

FIGURE 55.—Variation of side-force-due-to-yawing derivative with taper ratio for unswept hexagonal plan form; $B=2$; $Bm=BA(1+\lambda)/2(1-\lambda)$.

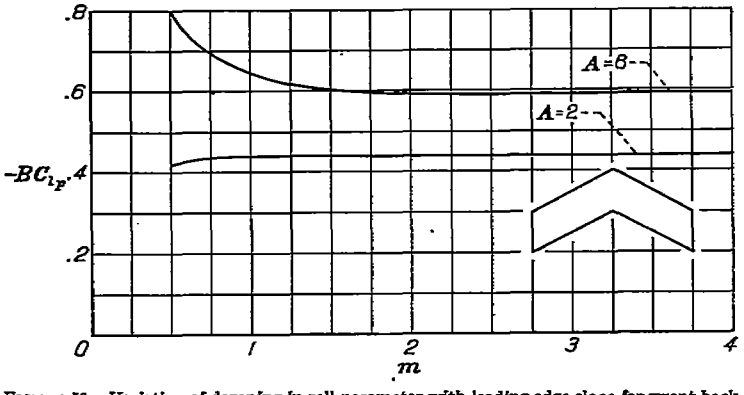

FIGURE 56.—Variation of damping-in-roll parameter with leading-edge slope for swept-back hexagonal plan form; $\lambda=1$; $B=2$.

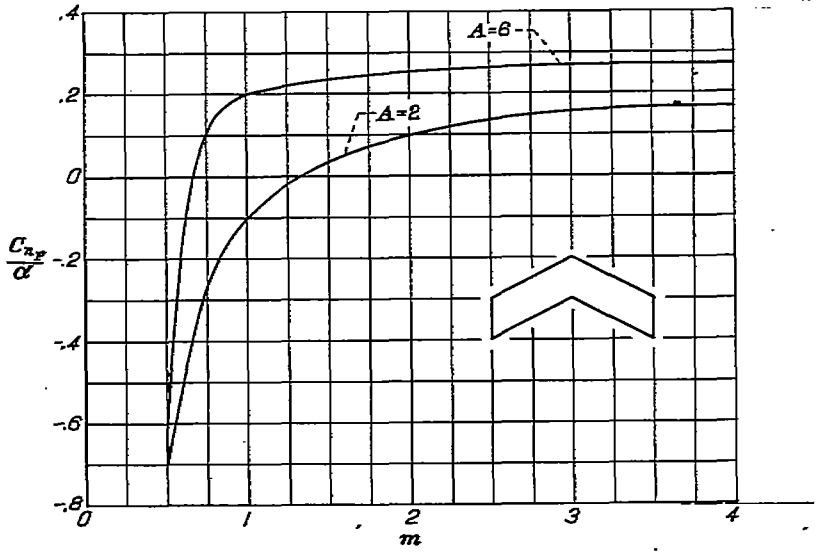

FIGURE 57.—Variation of yawing-moment-due-to-roll derivative with leading-edge slope for swept-back hexagonal plan form; $\lambda=1$; $B=2$.

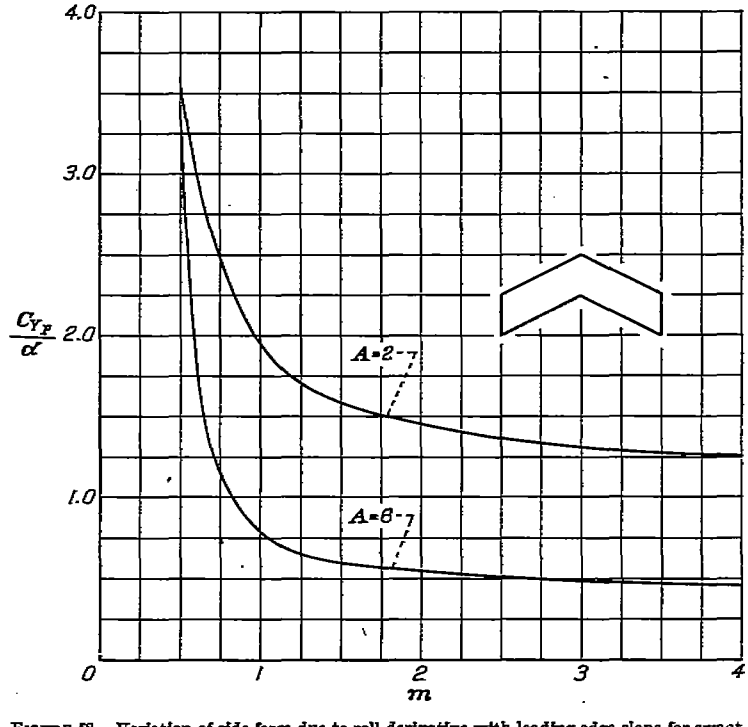

FIGURE 58.—Variation of side-force-due-to-roll derivative with leading-edge slope for swept-back hexagonal plan form; $\lambda=1$; $B=2$.

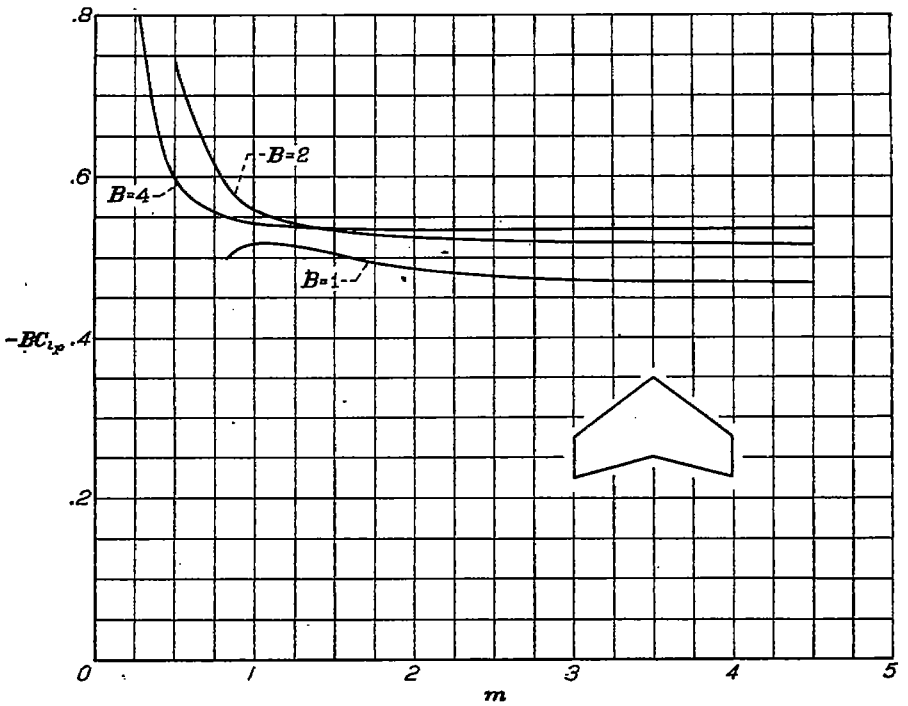

FIGURE 59.—Variation of damping-in-roll parameter with leading-edge slope for swept-back hexagonal plan form; $\lambda=0.5$; $A=6$.

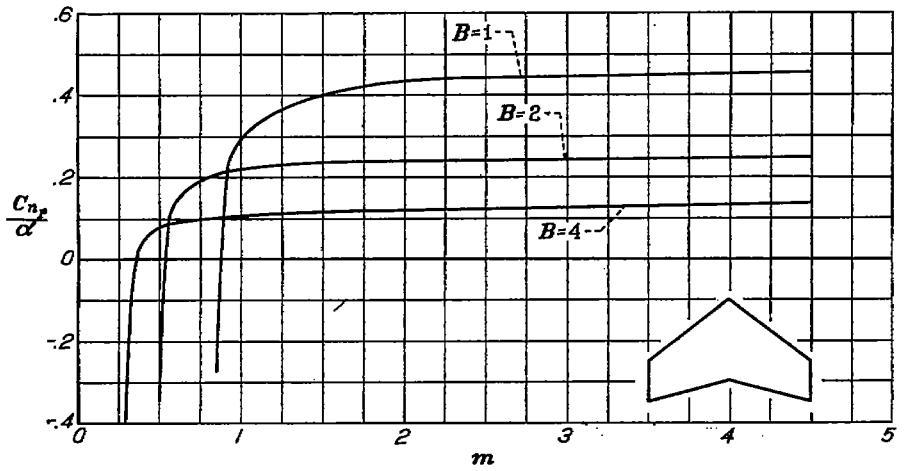

FIGURE 60.—Variation of yawing-moment-due-to-roll derivative with leading-edge slope for swept-back hexagonal plan form; $\lambda=0.5$; $A=6$.

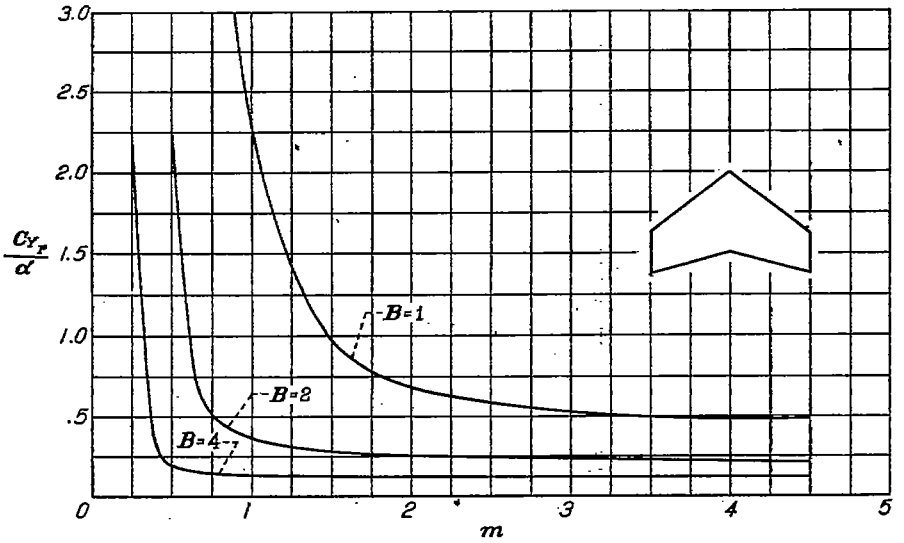

FIGURE 61.—Variation of side-force-due-to-roll derivative with leading-edge slope for swept-back hexagonal plan form; $\lambda=0.5$; $A=6$.

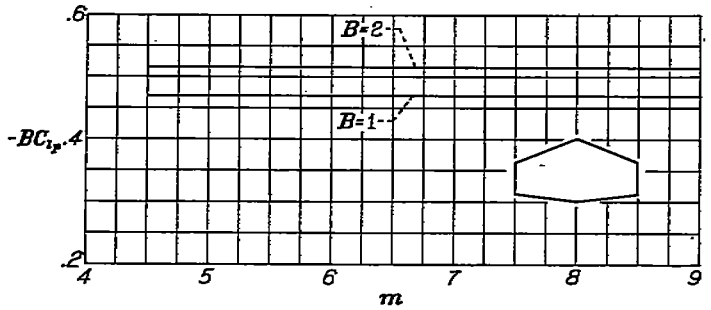

FIGURE 62.—Variation of damping-in-roll parameter with leading-edge slope for unswept hexagonal plan form; $\lambda=0.5$; $A=6$.

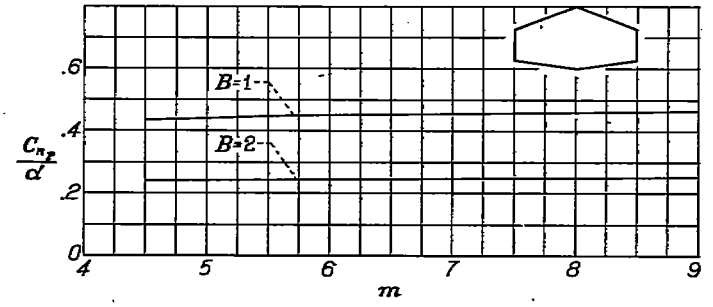

FIGURE 63.—Variation of yawing-moment-due-to-roll derivative with leading edge slope for unswept hexagonal plan form; $\lambda=0.5$; $A=6$.

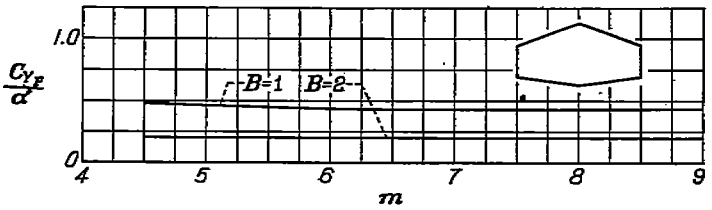

FIGURE 64.—Variation of side-force-due-to-roll derivative with taper ratio for unswept hexagonal plan form; $\lambda=0.5$; $A=6$.

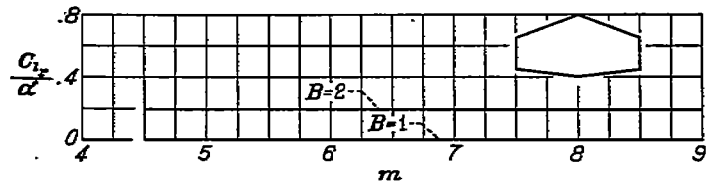

FIGURE 65.—Variation of rolling-moment-due-to-yawing derivative with leading-edge slope for unswept hexagonal plan form; $\lambda=0.5$; $A=6$.

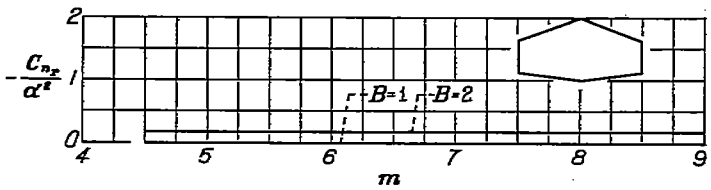

FIGURE 66.—Variation of damping-in-yaw derivative with leading-edge slope for unswept hexagonal plan form; $\lambda=0.5$; $A=6$.

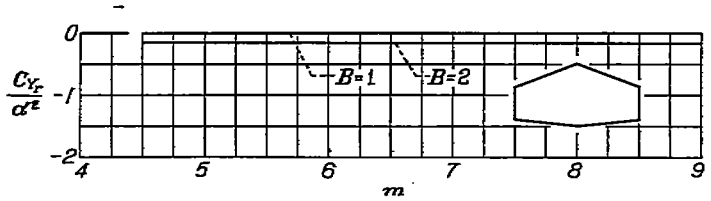

FIGURE 67.—Variation of side-force-due-to-yawing derivative with leading-edge slope for unswept hexagonal plan form; $\lambda=0.5$; $A=6$.